# Investigation of Fracture Properties of California Asphalt Concrete Mixtures

CALIFORNIA STATE UNIVERSITY
LONG BEACH
DEPARTMENT OF CIVIL ENGINEERING AND CONSTRUCTION ENGINEERING MANAGEMENT

Project No. 11-21

By

Shadi Saadeh, Ph.D.
Assistant Professor

and

Hamed Hakimelahi
Graduate Student

Department of Civil Engineering and Construction Engineering Management

California State University, Long Beach
1250 Bellflower Blvd, Long Beach, CA 90840

September 2012

## Disclaimer

The contents of this report reflect the views of the authors, who are responsible for the facts and the accuracy of the information presented herein. This document is disseminated under the sponsorship of the Department of Transportation, University Transportation Centers Program, and California Department of Transportation in the interest of information exchange. The U.S. Government and California Department of Transportation assume no liability for the contents or use thereof. The contents do not necessarily reflect the official views or policies of the State of California or the Department of Transportation. This report does not constitute a standard, specification, or regulation.

## Disclosure

This project was funded in its entirety under a contract with the California Department of Transportation.

## Acknowledgments

The authors would like to thank the United States Department of Transportation, the California Department of Transportation and METRANS for their interest and provision of grant support to make this project possible. We would also like to thank the University of California Pavement Research Center (Davis and Berkeley) for their invaluable technical and operational support of the project.

## ABSTRACT:

Fatigue cracking is a primary distress in asphalt concrete due to repetitive stresses and strains caused by both traffic loading and environmental factors. The fatigue resistance of AC has been investigated by a number of fatigue tests. The main objective of this study is to investigate the use of the semi-circular bend (SCB) test as a quality assurance/quality control (QA/QC) measure for field construction. SCB test parameters were determined using two methods, the first of which was cross-head movement, and the second was non-contact camera. Comparison of fracture properties of seven AC mixtures from the SCB CHM method and the beam-fatigue test (BFT) is made. The $J_c$ and $K_{1c}$ values for the seven mixtures were determined. BFT was performed on the same mixtures and initial stiffness, $N_f$ and PV were determined. The coefficient of variation (CV) ranged from 0 to 38% for $J_c$ and from 0 to 35% for $K_{1c}$. The coefficient of variation (CV) ranged from 10 to 93% for the initial stiffness, 2 to 83% for $N_f$, and 8 to 167% for PV. The SCB $J_c$ and BFT $N_f$ and PV indicated lower fracture properties for PG64-10RAP (LIME), AN-HMA and WMA-ADVERA mixtures than those of other mixtures. The BFT $N_f$ and PV achieved similar ranking for all mixtures. There is good correlation between $N_f$ and PV with $J_c$, and poor correlation between initial stiffness with $J_c$, $N_f$ and PV. This has indicated that the initial stiffness is not a good representative of the fracture properties of AC while $J_c$, $N_f$ and PV are better indicators. In addition, a comparison of the results of two method of measuring SCB test parameters on six AC mixtures indicated that there is good relation between the two SCB test methods. The results of this study indicate that the SCB test has great potential as a QA/QC test of fracture properties of asphalt mixtures.

# TABLE OF CONTENTS

## LIST OF FIGURES

# LIST OF TABLES

## 2. INTRODUCTION

Fatigue life resistance of asphalt concrete (AC) is defined as AC's ability to resist repeated traffic loading without significant cracking or failure [1]. Fatigue cracking is a primary distress in asphalt concrete that is caused by the repetitive stresses and strains due to traffic loading and environmental factors such as temperature differences. The fatigue resistance of AC is investigated by a number of fatigue tests.

Fatigue cracking occurs when the pavement has been stressed to the limit of its fatigue life by a repetitive axial load. Fatigue cracking is often associated with loads that are too heavy for pavement structure or more repetitions of a given load, which is provided for the design [2].

Wagoner et al. [4] developed the disk-shaped compact tension (DC(T)) test as a practical method for obtaining the fracture energy of asphalt concrete. Suitable specimen geometry was developed using the ASTM E399 standard for compact tension testing of metals. The fracture energy of the asphalt specimens can be calculated from this test. The variability of the fracture energy obtained from the DC(T) geometry was found to be comparable with the variability associated with other fracture tests for asphalt concrete.

Zhou et al. [5] presented the Texas overlay test (OT). The researchers at Texas Transportation Institute developed this test to assess the fatigue cracking prediction. In the test AC specimens that are glued to two steel plates, with half of the specimen's length resting on each plate. One of the steel plates is fixed and the other moves horizontally to simulate the opening and closing of the crack under overlays. The AC mixture specimen has a standard dimension of 150 mm length by 75 mm width by 38 mm height. The test specimen can be fabricated from a Superpave gyratory compactor (SGC) or from field cores.

Li et al. [6] conducted a comprehensive evaluation of HMA low-temperature cracking. The fracture resistance properties of 28 asphalt mixtures combining different factors such as binder type, binder modifier, aggregate type, air voids, and asphalt content were evaluated with the SCB test configuration. Each mix was tested at three different temperatures. Three replicates were tested at each temperature for all mixtures. The test temperatures were determined based on the asphalt binder performance grade (PG) lower limit: Temperature 1 = binder PG low limit +10°C; Temperature 2 = Temperature 1 – 12 °C; Temperature 3 = Temperature 1 + 12 °C. Experimental data were analyzed and statistical analyses were conducted to evaluate the effects of various factors on the fracture resistance of the asphalt mixtures tested. The authors raised the point that linear elastic fracture mechanics (LEFM) assumptions are not valid for SCB specimens as well as the material under investigation. Statistical analyses were performed to evaluate the significance of the different factors on mixture low-temperature cracking resistance. The factors considered were aggregate type, air voids, asphalt content, modifier type, and binder type. ANOVA with a 95% level of confidence showed that the test temperature had a significant effect on both fracture energy and fracture toughness. Fracture energy increased and fracture toughness decreased as the test temperature increased, indicating a change in mixture behavior from brittle to brittle-ductile behavior.

Chingmai et al. [7] examined the relation between fatigue and fracture parameters obtained from standardized laboratory tests. Two fatigue parameters, number of cycles to failure and plateau value (PV), were obtained from flexural bending test. The Disk-shaped compact tension DC(T) fracture test was used to obtain fracture energy parameters, including fracture strength, pre-peak fracture energy, post-peak fracture energy, and total fracture energy. The correlations between fatigue and fracture parameters indicated that the plateau value (PV) has a better relationship with fracture parameters than the traditional fatigue criteria ($N_{f50}$). Also,

results indicated an inverse trend between fatigue and fracture parameters at low strain levels such as 300 micro-strains in comparison with high strain levels, 700 and 1000 micro-strain.

In California, the Asphalt Research Program performed a five-year study on the fatigue performance of AC mixtures, Harvey et al. [1]. To predict fatigue performance of asphalt mixtures, Beam Fatigue Test (BFT) was developed during this study. BFT requires long testing period and can't be run on the field which makes BFT impractical for QC/QA testing.

This study was therefore motivated by the desire to investigate the feasibility of predicting time-consuming BFT results with SCB test results. The reason the SCB test is chosen in this study is that it is simple to conduct (a regular stabilometer can be used to conduct the test), inexpensive (one compacted specimen makes four SCB specimens), simple to analyze (the output parameter is indicative of the dissipated energy during the crack propagation), and the failure mode of SCB is due to tensile stress induced by bending.

During the 1990s, a simple test (SCB) was developed to determine the crack resistance and crack growth rate of bituminous mixtures. In recent years the SCB test has become a popular way to determine fracture toughness of HMA. Hofman and his group found that the cyclic SCB test is very promising for determining the Paris constants [8].

Saadeh et al. [9] investigated the influence of moisture on fracture properties of asphalt mixtures. Twenty-four SCB tests were conducted on two California asphalt mixtures in dry and wet conditions. In addition, 16 BFT were conducted on the same HMA mixtures in dry and wet conditions. The results of these two tests were compared. The data analysis showed that there is a good relation between BFT and SCB however; they recommended more tests should be done on more AC mixtures in order to get reliable results.

The SCB test has recently been used in many pavement material researches to investigate the fracture properties of HMA mixtures [10, 11, 12, 13 and 14]. The SCB test can be a potential test to further exploration of the material fracture properties.

Molenaar et al. [15] studied the effectiveness of SCB to characterize asphalt mixtures using a finite element (FE) model that was developed to calculate tensile and compression stresses "that occur in SCB samples during testing. The FE software CAPA-3D was used to run the simulations. The analysis revealed that the dominant failure mode in the SCB test is cracking due to tension stresses. Thus, the test gives relevant information on the tensile characteristics of the asphalt mixes tested. The authors concluded that SCB is a simple, low cost test that can be easily performed on specimens prepared by means of a gyratory compactor or on specimens taken from pavements. It was concluded by the authors that the SCB test can be a very useful tool in mixture design and for QA/QC purposes.

Li and Marasteanu [16] used the cohesive zone model (CZM) technique to describe the fracture behavior of asphalt mixtures at low temperatures. CZM was adopted to describe the local material behavior around the crack tip using a zero-thickness interface element, and the performance of this interface element was tested with analytical solutions on an elastic double cantilever beam. The FE simulation was calibrated with experimental results from an SCB test. The authors concluded that the model has the potential to effectively simulate the fracture in asphalt pavements at low temperatures.

In this study, an experimental and numerical evaluation of the SCB test is conducted. A comprehensive comparison of BFT and SCB test parameters was conducted. In addition, an advanced FE modeling approach called eXtended finite element method (XFEM) is used to numerically simulate the SCB test process. This study, to the best knowledge of the authors, is the first to investigate the SCB test using XFEM. The SCB test and modeling results of this study are being considered for use as a QC/QA test for construction projects incorporating performance-related materials specifications based on designs performed using a mechanistic

empirical pavement design method called CalME that is currently being developed by Caltrans and the University of California Pavement Research Center (UCPRC).

.

## 3. OBJECTIVE

The objective of this study is to investigate the use of the semi-circular bend (SCB) test as a QA/QC measure for field construction and to investigate the feasibility of using SCB test results as a trigger for further investigation using BFT. This objective was achieved by testing seven asphalt mixtures including mixtures with recycled asphalt pavement (RAP), warm mix asphalt (WMA), lime, and polymer modified asphalt. Part of the experimental program results were used to develop and calibrate an FE model of the SCB test. The model was then used to investigate crack propagation in SCB and to predict SCB simulations for experimental results not used in the calibration process.

.

## 4. SCOPE

Seven AC mixture types (PG64-10RAP [LIME], PG64-28PM [LIME], 710P4-AR, AN-HMA, AN-WMA, MnROAD, and WMA-ADVERA) that are widely used in California were investigated in this study.

BFT and SCB tests were conducted to investigate the performance of AC mixtures. The fracture properties of AC mixtures were determined by these two tests. The crack length propagation was estimated using two methods, the first of which was the cross-head movement and the second of which was the use of non-contact camera. The same specifications and methodology was used to prepare cores for SCB testing and beams for BFT. The SCB test was performed at California State University Long Beach and BFT was conducted at University of California Pavement Research Center.

# 5. METHODOLOGY

In this study, the use of SCB test as QA/QC test to trigger further investigation of the fracture properties of asphalt mixtures using BFT is investigated. To achieve this goal, six different AC mixtures used in California and one from MinRoad are selected. Various asphalt mixtures with various gradation and mixture designs were selected to achieve a comprehensive comparison and evaluation.

## 5.1. Material Properties and Mixture Design

A total of 42 SCB CHM methods and 21 BFTs were conducted on seven asphalt mixtures (PG64-10RAP [LIME], PG64-28PM [LIME], 710P4-AR, AN-HMA, AN-WMA, MnROAD, WMA-ADVERA) that are used in California. In addition 18 SCB camera-method tests were conducted on the same mixtures (with the exception of MnROAD). For the SCB specimens, three notch depths (1", 1.25" and 1.5") were used. Rolling wheel was the method of compaction used. A similar compaction method was used to prepare BFT specimens.

Table 1 provides information about the mixture properties that were used in this study. As presented in Table 1, two methods of mix design, SHRP Level 1 and Caltrans' type A_19mm methods were used. Samples were fabricated using two methods: lab-mixed lab-compacted and field mixed field compacted. As can be seen in table 1, aggregates are provided from different places and the rice specific gravity value ranged between 2.457 to 2.596.

The gradation for PG64-10RAP (LIME) and PG64-28PM (LIME) mixtures is provided in Figure 1. The mixture with 25% RAP was named PG64-10RAP (LIME) and the mixture with 0% RAP is was named PG64-28PM (LIME). For the 710P4-AR, AN-HMA, AN-WMA, WMA-ADVERA mixtures Caltrans' HMA-A_19mm section 39 specifications was used foraggregate gradation. Figure 2 shows the lower and upper limit for aggregate gradation based on Caltrans' HMA-A_19mm.

**TABLE 1, HMA Mixtures Properties**

| Mix Type | Binder Type | Specimen Designation | Mix Design | Aggregate Source | Specimen Preparation Type | RICE |
|---|---|---|---|---|---|---|
| **PG64-10RAP (Lime)** | PG64-10 (Valero) | 3.15-RAP-6410-5.38-1C2 | SHRP Level 1 mix design | Red Bluff (District 2) | LMLC[1] | 2.4578 |
| | | 3.15-RAP-6410-5.38-2A1 | | | | |
| | | 3.15-RAP-6410-5.38-3C1 | | | | |
| **PG64-28PM (Lime)** | PG64-28PM (Valero) | 3.15-ME-6428PM-5.2-3D1 | SHRP Level 1 mix design | Red Bluff (District 2) | LMLC | 2.489 |
| | | 3.15-ME-6428PM-5.2-4B1 | | | | |
| | | 3.15-ME-6428PM-5.2-5B2 | | | | |
| **710P4-AR** | AR-8000 paving asphalt (AASHTO MP1 designation PG64-16) | 710P4-AR8-4.8-2D1 | Caltrans' HMA-A_19mm | San Gabriel River Valley at Azusa | LMLC | 2.555 |
| | | 710P4-AR8-4.8-10D1 | | | | |
| **AN-HMA** | PG64-10 (Valero-Benicia) | AN-WMA-DG-6B1 | Caltrans' HMA-A_19mm | Graniterock-Wilson Quarry | LMLC | 2.575 |
| | | AN-WMA-DG-10B2 | | | | |
| | | AN-WMA-DG-14B2 | | | | |
| **AN-WMA** | PG64-10 (Valero-Benicia) | AN-WMA-13A1 | Caltrans' HMA-A_19mm | Graniterock-Wilson Quarry | LMLC | 2.576 |
| | | AN-WMA-32B2 | | | | |
| | | AN-WMA-35A1 | | | | |
| **MnROAD** | | MN281C2 | | | FMFC[2] | 2.516 |
| | | MN282D1 | | | | |
| | | MN2410D2 | | | | |
| **WMA-ADVERA** | PG64-16 (Valero-Benicia) | WMA-A33-1B | Caltrans' HMA-A_19mm | Graniterock-Wilson Quarry | FMFC | 2.596 |
| | | WMA-A33-2B | | | | |
| | | WMA-A33-3B | | | | |

1. Lab-Mixed Lab-Compacted
2. Field Mixed Field Compacted

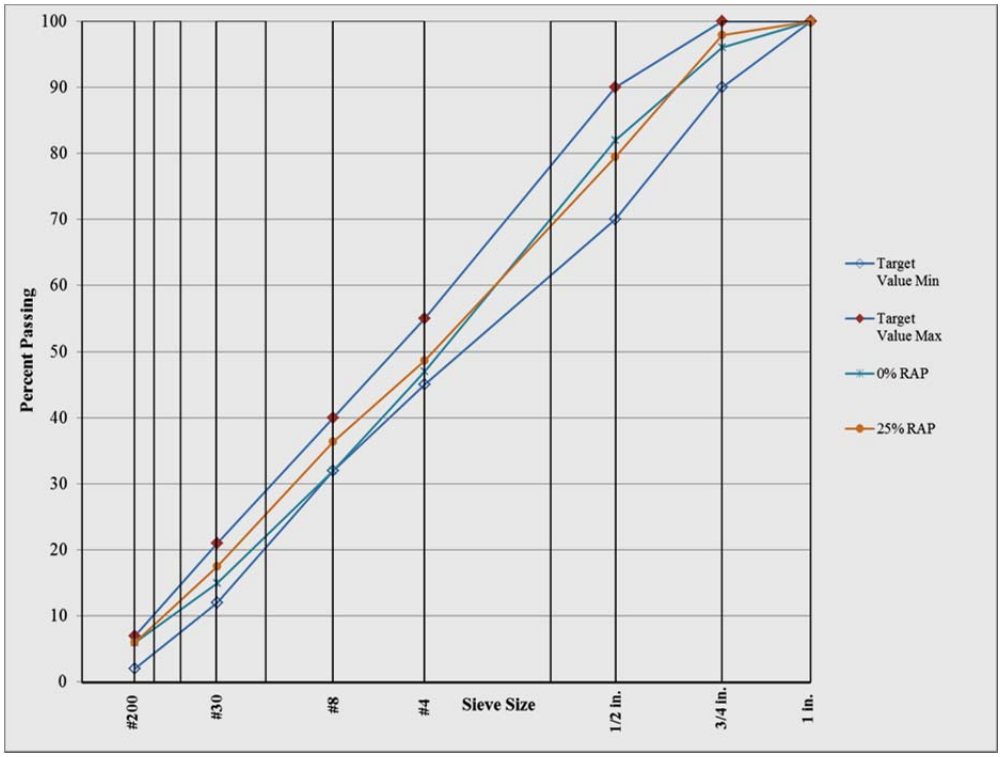


**FIGURE 1, PG64-10RAP (LIME) (25% RAP) and PG64-28PM (Lime) (0% RAP) Gradation**

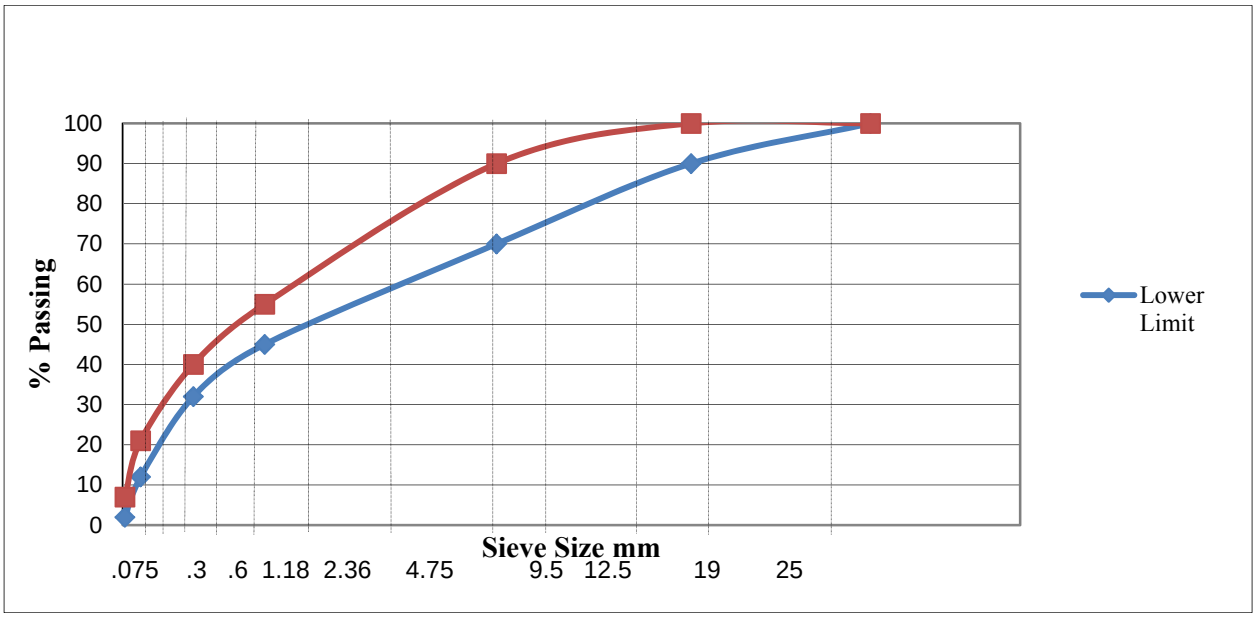


**FIGURE 2, Gradation Limits for Caltrans' HMA-A_19mm**

## 5.2. Testing Factorial:

Seven different AC mixtures were used in this study and a specific name was designated to each mixture replicate. Both BFT and SCB tests were conducted at 20 °C. In the SCB test, the monotonic loading deformation rate was 0.5 mm/min. (0.02 in/min), and the BFT was conducted at the strain level of 400 micro-strains. Tables 2 and 3 present test factorial for the BFT and SCB test, respectively. A description of each test is provided below.

**TABLE 2, BFT Factorial**

| Mix Type | Specimen Designation | AV (%) | AC (%) | Test Temp. (°C) | Test Strain Level |
|---|---|---|---|---|---|
| **PG64-10RAP (LIME)** | 3.15-RAP-6410-5.38-1C2 | 5.9 | 5.38 | 19.89 | 0.000405 |
| | 3.15-RAP-6410-5.38-2A1 | 5.7 | 5.38 | 19.78 | 0.000406 |
| | 3.15-RAP-6410-5.38-3C1 | 6.1 | 5.38 | 19.87 | 0.000406 |
| **PG64-28PM (LIME)** | 3.15-ME-6428PM-5.2-3D1 | 5.8 | 5.2 | 19.96 | 0.000411 |
| | 3.15-ME-6428PM-5.2-4B1 | 5.5 | 5.2 | 19.83 | 0.000414 |
| | 3.15-ME-6428PM-5.2-5B2 | 5.7 | 5.2 | 19.84 | 0.000408 |
| **710P4-AR** | 710P4-AR8-4.8-2D1 | 5.5 | 4.8 | 20.44 | 0.000416 |
| | 710P4-AR8-4.8-10D1 | 4.8 | 4.8 | 20.62 | 0.000414 |
| **AN-HMA** | AN-WMA-DG-6B1 | 4.6 | 5.2 | 20 | 0.000399 |
| | AN-WMA-DG-10B2 | 4.4 | 5.2 | 20.1 | 0.000395 |
| | AN-WMA-DG-14B2 | 5 | 5.2 | 20.35 | 0.000414 |
| **AN-WMA** | AN-WMA-13A1 | 4.8 | 5.2 | 19.95 | 0.000394 |
| | AN-WMA-32B2 | 4.9 | 5.2 | 19.92 | 0.000397 |
| | AN-WMA-35A1 | 4.5 | 5.2 | 19.63 | 0.000402 |
| **MnROAD** | MN281C2 | 6.1 | | 20.02 | 0.000404 |
| | MN282D1 | 7 | | 20.01 | 0.000403 |
| | MN2410D2 | 7 | | 20 | 0.000405 |
| **WMA-ADVERA** | WMA-A33-1B | 7.8 | 5.2 | 19.75 | 0.000404 |
| | WMA-A33-2B | 8.1 | 5.2 | 19.81 | 0.000404 |
| | WMA-A33-3B | 10.3 | 5.2 | 19.84 | 0.000405 |

**TABLE 3, SCB Test Factorial**

| Mix Type | Specimen Designation | | Notch Size | AV (%) |
|---|---|---|---|---|
| PG64-10RAP (LIME) | 3.15-HAM-RAP-64-10-5.38-1-1D | A | 25.40 | 4.90 |
| | 3.15-HAM-RAP-64-10-5.38-1-1D | B | 25.40 | |
| | 3.15-HAM-RAP-64-10-5.38-1-2C | A | 31.75 | 5.50 |
| | 3.15-HAM-RAP-64-10-5.38-1-2C | B | 31.75 | |
| | 3.15-HAM-RAP-64-10-5.38-2-1C | A | 38.10 | 4.70 |
| | 3.15-HAM-RAP-64-10-5.38-2-1C | B | 38.10 | |
| PG64-28PM (LIME) | 3.15-PG64-28PM-5.2-1-2C | A | 25.40 | 5.20 |
| | 3.15-PG64-28PM-5.2-1-2C | B | 25.40 | |
| | 3.15-PG64-28PM-5.2-1-3C | A | 31.75 | 5.10 |
| | 3.15-PG64-28PM-5.2-1-3C | B | 31.75 | |
| | 3.15-PG64-28PM-5.2-2-3C | A | 38.10 | 4.90 |
| | 3.15-PG64-28PM-5.2-2-3C | B | 38.10 | |
| 710P4-AR | 710p4-AR-4.3-1-2C | A | 25.40 | 6.10 |
| | 710p4-AR-4.3-1-2C | B | 25.40 | |
| | 710p4-AR-4.3-1-3C | A | 31.75 | 6.10 |
| | 710p4-AR-4.3-1-3C | B | 31.75 | |
| | 710p4-AR-4.3-2-2C | A | 38.10 | 6.30 |
| | 710p4-AR-4.3-2-2C | B | 38.10 | |
| AN-HMA | AN-WMA-DG-8-2B | A | 25.40 | 4.60 |
| | AN-WMA-DG-8-2B | B | 25.40 | |
| | AN-WMA-DG-8-3B | A | 31.75 | 3.90 |
| | AN-WMA-DG-8-3B | B | 31.75 | |
| | AN-WMA-DG-9-3A | A | 38.10 | 6.30 |
| | AN-WMA-DG-9-3A | B | 38.10 | |
| AN-WMA | AN-WMA-2-1B | A | 25.40 | 6.00 |
| | AN-WMA-2-1B | B | 25.40 | |
| | AN-WMA-6-1B | A | 31.75 | 6.60 |
| | AN-WMA-6-1B | B | 31.75 | |
| | AN-WMA-6-2B | A | 38.10 | 6.90 |
| | AN-WMA-6-2B | B | 38.10 | |
| MnROAD | 3.4-MIN II-9-1D | A | 25.40 | 5.30 |
| | 3.4-MIN II-9-1D | B | 25.40 | |
| | 3.4-MIN II-9-2D | A | 31.75 | 4.30 |
| | 3.4-MIN II-9-2D | B | 31.75 | |
| | 3.4-MIN II-9-3D | A | 38.10 | 4.90 |
| | 3.4-MIN II-9-3D | B | 38.10 | |
| WMA-ADVERA | WMA-A3-4T | A | 25.40 | 9.10 |
| | WMA-A3-4T | B | 25.40 | |
| | WMA-A18-4C | A | 31.75 | 8.70 |
| | WMA-A18-4C | B | 31.75 | |
| | WMA-A31-8C | A | 38.10 | 8.40 |
| | WMA-A31-8C | B | 38.10 | |

## 6. Semi-Circular Bend (SCB) Test

The SCB test is used to characterize the fracture resistance of asphalt mixtures based on a fracture mechanics concept. In this study, SCB test parameters were measured based on two methods that followed the same concept. The critical strain energy release rate, which is called the critical value of J-integral or $J_c$ was determined for each mixture tested. Fracture toughness ($K_{1c}$) is another parameter that was determined according to Hafman et el. [8]. In this test, semi-circular samples with three notch depths of 1, 1.25, and 1.5 inches (25.4, 31.75 and 38.1 mm) are used and the scheme of a typical test specimen is shown in figure 3. The tests were conducted at 20 °C.

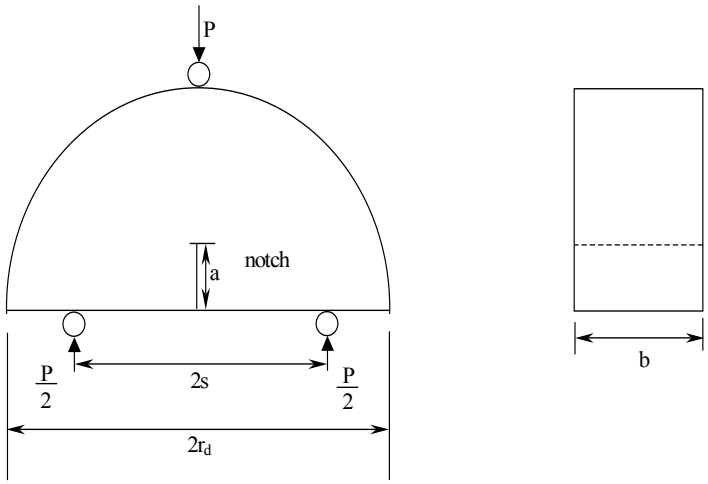


**FIGURE 3, SCB Test Specimen Scheme**

### 6.1. SCB Test- Cross-head Movement Method

In the SCB cross-head movement method, the specimens were loaded monotonically until fracture under a constant cross-head deformation rate of 0.02 in/min in a three-point bend load configuration as shown in figure 4. The maximum load ($F_{max}$), on the load-deformation curve was determined. The load and deformation was continuously recorded and the critical value of J-integral and $K_{1c}$ were determined using the following equations:

$$J_c = -\left(\frac{1}{b}\right)\frac{\partial U}{\partial a} \quad [1]$$

Where "b" is sample thickness, "a" is the notch depth, and "U" is the strain energy to failure

$$\sigma_{max} = \frac{4.263.F_{max}}{D.t} \quad [2]$$

$$K_{1c} = \sigma_{max}\sqrt{\pi a} f\left(\frac{a}{W}\right) \quad [3]$$

Where

$$f\left(\frac{a}{W}\right) = -0.623 + 29.29\left(\frac{a}{W}\right) - 171.2\left(\frac{a}{W}\right)^2 + 457.1\left(\frac{a}{W}\right)^3 - 561.2\left(\frac{a}{W}\right)^4 + 265.54\left(\frac{a}{W}\right)^5$$

And "$\sigma_{max}$" is the maximum stress, "$F_{max}$" is the maximum load, "$K_{1c}$" is fracture toughness, "a" is the initial notch depth and "W" is the specimen's height. Hofman et al. [6] determined the correlation factor "f" through 2D finite element analysis.

**FIGURE 4, SCB Test- Cross-Head Movement Method**

## 6.2. SCB Test- Camera Method

During the SCB test, a non-contact camera was fixed in front of the SCB specimen to measure the crack length, which is named SCB test- camera method. This method of measuring crack length is highly reliable. The camera system (ARAMIS) is provided by Trilion Optical Test Systems, Figure 5. This method was used on the same specimens (simultaneously) that were analyzed using SCB CHM. The only difference is the way of measuring crack length.

ARAMIS is a powerful optical system for measurement of complex materials and structures to determine their 3D deformation and strain during loading. This tool is a highly robust, full-field, non-contact strain measuring testing device. The system offers a non-contact measurement of 3D deformation and strain using 3D image correlation methods (digital image correlation, DIC) using high-resolution digital CCD cameras.

The camera used in this study made it possible to measure the irregular crack length at different stages of the test, Figure 6. For each of the 18 specimens, the crack length in different stages was measured. This technique was developed jointly with the Trilion Company.

In the SCB Camera method, the specimens were loaded monotonically until fracture under a constant cross-head deformation rate of 0.02 in/min in a three-point bend load configuration as shown in Figure 3. The maximum load ($F_{max}$), J-integral and $K_{1c}$ were determined as described in the previous section. The results from the irregular crack measurement were compared to the cross-head movement. The comparison of these parameters provides better understanding of the SCB test and helps to provide accurate measurement of the crack length.

**FIGURE 5, SCB Test-Camera Method**

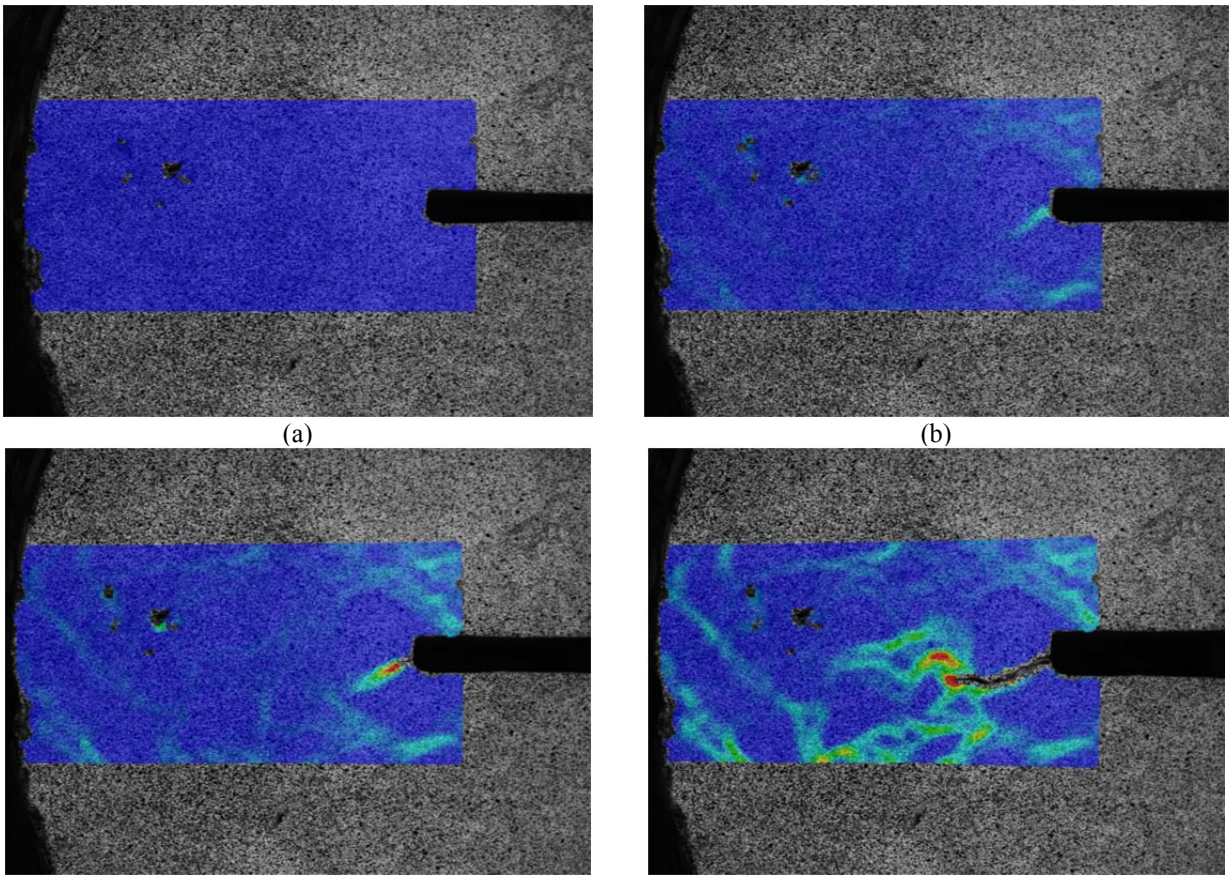

(a) (b)

(c) (d)

**FIGURE 6, SCB Test-Camera Method Procedure**
**(a) Stage 1, (b) Stage 25, (c) Stage 38, (d) Stage 58**

## 7. Beam Fatigue Test (BFT)

This test was conducted according to AASHTO T-321. The test was conducted at a strain level of 400 micro-strains and temperature of 20 °C. In this study, BFTs were conducted based on controlled strain method. Figure 7 shows the fatigue beam test device. This device is capable of applying sinusoidal loading with the controlled level of strain. The device also provides the ability to control the test temperature. In this study, BFTs were performed at the University of California Pavement Research Center.


**FIGURE 7, Fatigue Beam Test (Courtesy of Inopave Inc.)**

In a BFT, the number of load cycles to failure ($N_{f,50}$) is determined as the number of cycles for a 50% reduction in initial stiffness (AASHTO Designation: T 321-03). $N_{f,50}$ can be calculated using the following equation:

$$N_{f,50} = \frac{\ln\left[\frac{S_{f,50}}{A}\right]}{b} \tag{4}$$

Where:

$S_{f,50}$= 50% reduction in initial stiffness

$A$= constant

$b$= constant

Another parameter that is used to evaluate fracture properties of AC mixtures is dissipated energy. Dissipated energy is the area under stress-strain curve of a hysteresis loop, Figure 8, and can be computed through the following equation:

$$W_i = \Pi \sigma_i \epsilon_i \sin \phi_i \tag{5}$$

Where:

$W_i$= dissipated energy at load cycle $i$,
$\sigma_i$= stress amplitude at load cycle $i$,
$\epsilon_i$= strain amplitude at load cycle $I$, and
$\phi_i$= phase angle between stress and strain wave signals.

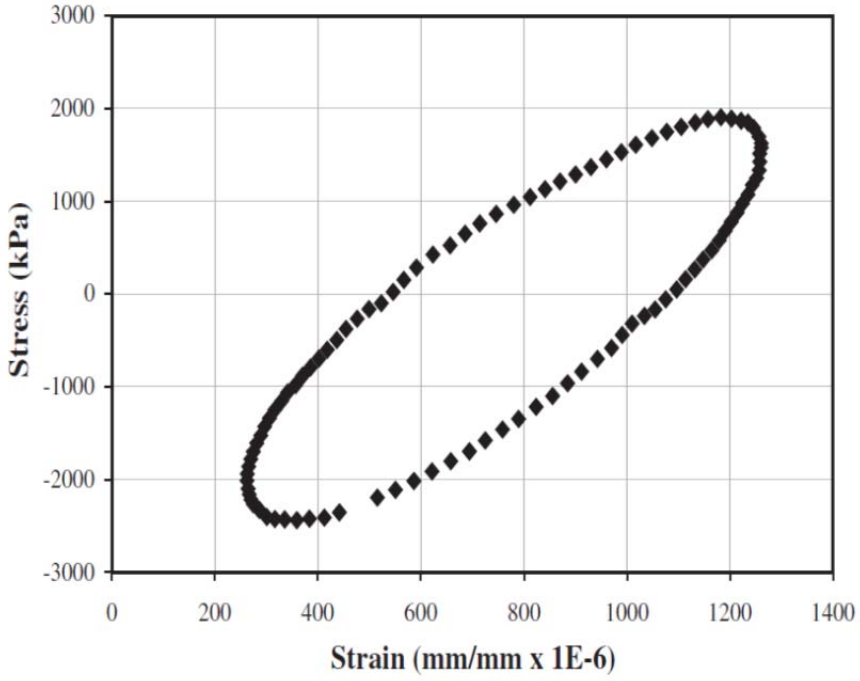


**FIGURE 8, Stress-Strain Hysteresis Loop (Ghuzlan and Carpenter 2000)**

In 1997, Carpenter and Jansen [17] introduced the change in dissipated energy to investigate fatigue behavior of HMA. Ghuzlan and Carpenter (2000) [18] used ratio of dissipated energy (RDEC) as an energy approach to describe fatigue damage. They proposed that a better indication of damage is provided by considering damage as a change in dissipated energy between two load cycles instead of considering it as the cumulative dissipated energy. RDEC can be calculated based on Equation 6. The definition shows the change in damage from one cycle to another. In this equation, the typical cycles between "b" and "a" is 100 and this number can be higher if the DE between 100 load cycles is low [19].

$$RDEC_a = \frac{DE_a - DE_b}{DE_a * (b-a)} \quad (6)$$

Where:
$a$, $b$ = loading cycle (LC) a and b, respectively (KPA);
$RDEC_a$ = average ratio of dissipated energy change at cycle a, compare to the nest cycle b;
$DE_a$, $DE_b$ = dissipated energy at load cycle a and b

The damage curve that describes the relation between RDEC and the number of cycles to failure is shown in Figure 9. Shen and Carpenter (2007) [19] divided the curve in three stages: the initial stage (stage I), the damage growth stage (stage II) and the stage at which damage grows rapidly (stage III). They proposed that the RDEC value lies at the 50% stiffness reduction point, and they defined this as the plateau value (PV), Figure 9.

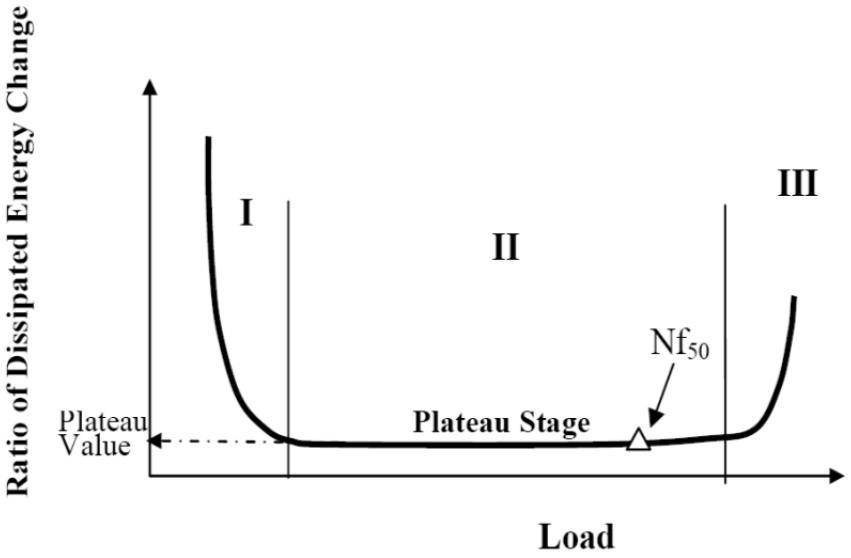


**FIGURE 9, Typical RDEC vs. Loading Cycles Plot and the Indication of PV and $Nf_{50}$ (Shen and Carpenter, 2007)**

Shen and Carpenter (2007) provided an equation to calculate PV, Equation 7. They also proposed a simplified equation to calculate PV for low strain fatigue testing, Equation 8.

$$PV = \frac{1-(1+\frac{100}{Nf_{50}})^{k}}{100} \tag{7}$$

$$PV = -\frac{k}{Nf_{50}} \tag{8}$$

Where
K= slope of the DE-LC curve

# 8. DISCUSSION OF RESULTS

## 8.1. Semi-Circular Bend (SCB) Test, Cross-Head Movement Method (CHM)

A total of 42 SCB tests were performed based on cross-head movement method on seven mixtures (PG64-10, PG64-28, 710P4-AR, AN-HMA, AN-WMA, MnROAD and WMA-ADVERA) with three notch-depths (1, 1.25 and 1.5 inch), and two replicates each.

Figure 10 presents the load-displacement curves for three notch depths of HMA mixtures that were used in this study. The maximum load ($F_{max}$) was recorded and the area under the load displacement curve was used to determine the strain energy (U).

The calculated strain energy for each notch was used to determine the critical strain energy $J_c$, Figure 11. This figure presents the strain energy verses notch depths for each AC mixture, and indicates a decrease in strain energy with the increase in the notch depth. By dividing the slope of the linear fitting line to the spaceman's thickness, the $J_c$ value can be calculated. The calculated peak load and the dissipated energy for each SCB test were used to determine the critical $K_{1c}$ and $J_c$ values, Equations 1 and 2.

The SCB CHM $J_c$ and $K_{1c}$ values for each AC mixture are presented in Tables 4 and 5, respectively. The tables present the dissipated energy (U), coefficient of variation (CV), the critical value of the J-integral ($J_c$), and the ranking of the mixtures based on the $J_c$ and $K_{1c}$ parameters. The values of $J_c$ ranged from 0.66 to1.198 kN.m (7.9 to14.4 lb.in). The values for $K_{1c}$ ranged from 1.7 to 4.4 N /$m^2$. The coefficient of variation ranged from 0 to 38% for $J_c$ and from 0 to 35% for $K_{1c}$.

In order to better compare the ranking of each parameter, the analysis of variance (ANOVA) was used. Using ANOVA, the P-value is used to determine whether the model is significant or not. Typically P is compared to an alpha value of 0.05. A P-value that is lower than alpha indicates that the model is significant. The Tukey analysis, which is a part of ANOVA, was used to examine the difference in the groups with different rankings.

The ANOVA results for the $J_c$ values are presented in tables (6a) and (7a) with 95% and 80% degree of confidence respectively. The Tukey analysis for the $J_c$ values is presented in tables (6b) and (7b) with 95% and 80% degree of confidence respectively.

The Tukey analysis with 95% degree of confidence that was done on $J_c$ values indicates that $J_c$ values can be categorized in just one group, Table (6b). In order to compare test results, more than one group of test results is needed. Therefore, ANOVA for $J_c$ values was done with 80% degree of confidence, table (7b). As a result, $J_c$ values were categorized in three separate groups. The compression of these three groups, with the mixtures' $J_c$ ranking, indicates that there is a direct correlation between the $J_c$ values which ranked (1 and 2), (3 and 4), (5, 6 and 7) in Table (4) and these three groups.

Similar to $J_c$, ANOVA was performed on $K_{1c}$ values with 95% degree of confidence and is presented in Table (8a). The P-value of 0 indicated that $K_{1c}$ is a significant parameter. Tukey analysis shows that the results for this parameter are categorized in five different groups, Table (8b).

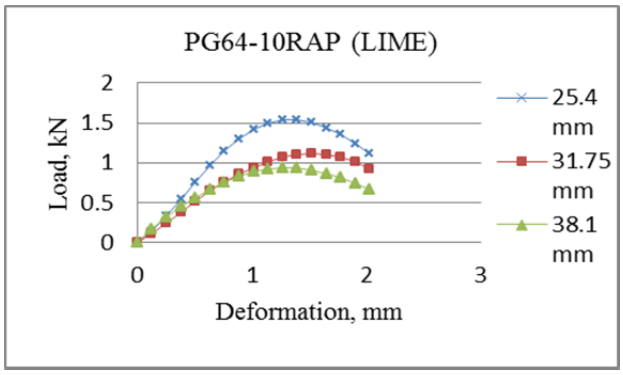


(a)

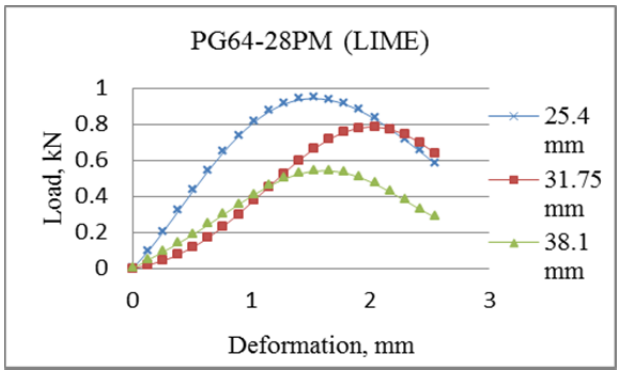


(b)

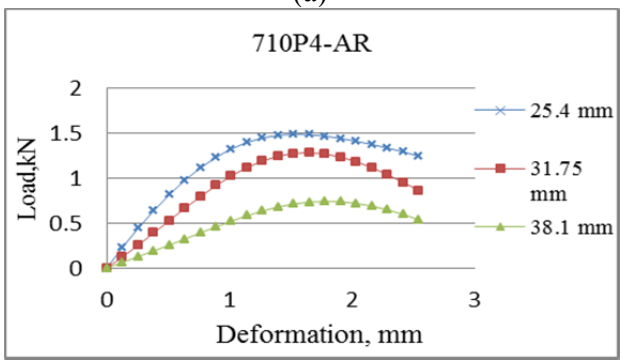


(c)

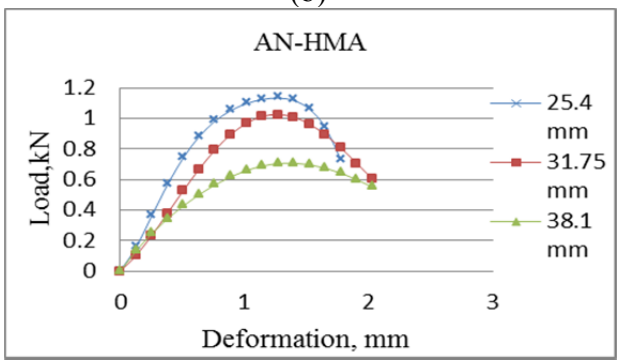


(d)

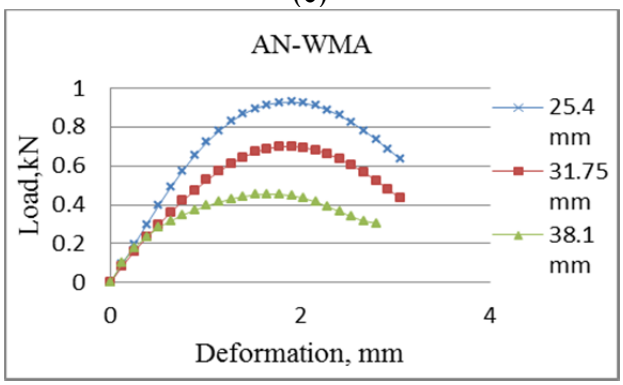


(e)

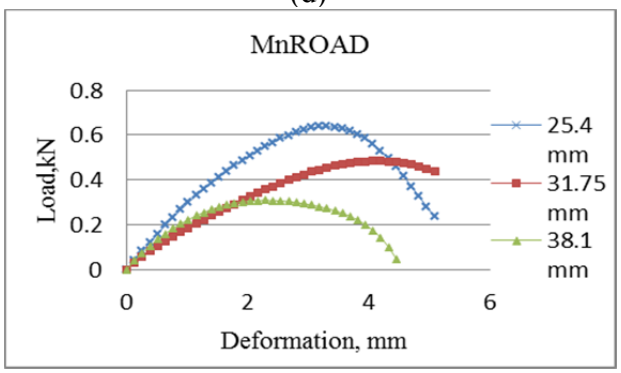


(f)

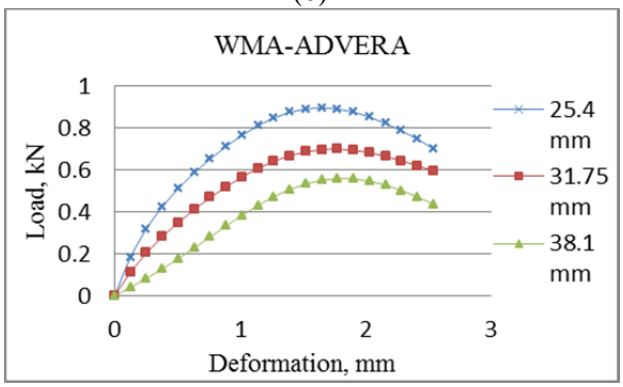


(g)

**FIGURE 10, Load-Deflection Curves of Modified HMA Mixtures (a) PG64-10RAP (b) PG64-28PM (c) 710P4-AR (d) AN-HMA (e) AN-WMA (f) MnROAD (g) WMA-ADVERA**

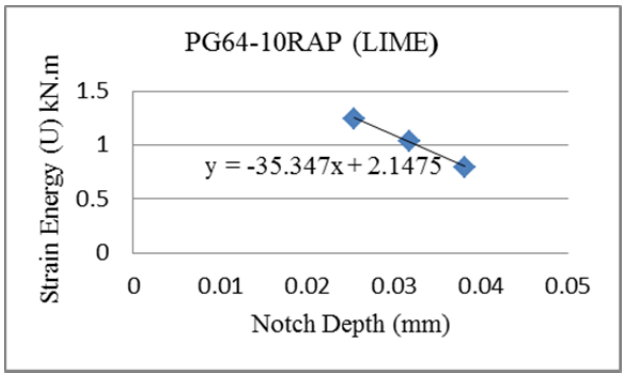


(a)

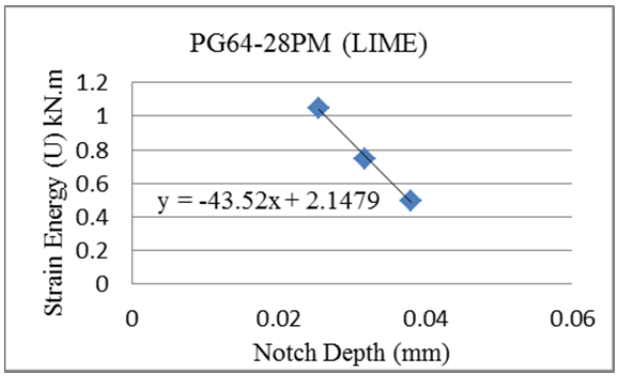


(b)

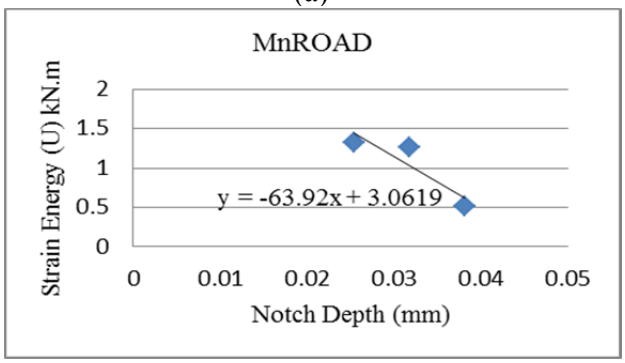


(c)

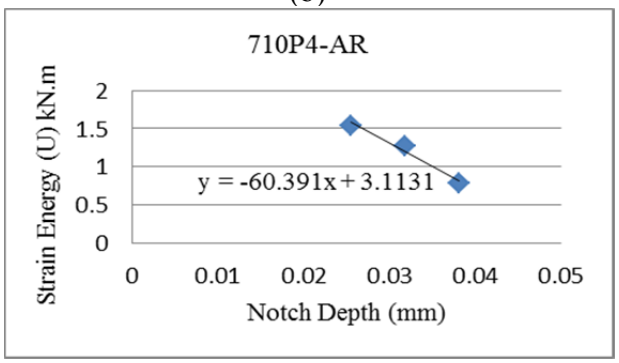


(d)

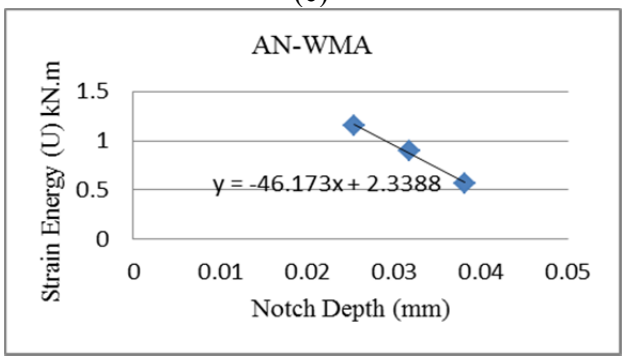


(e)

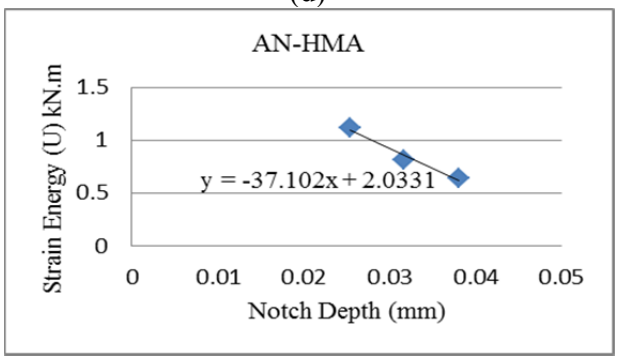


(f)

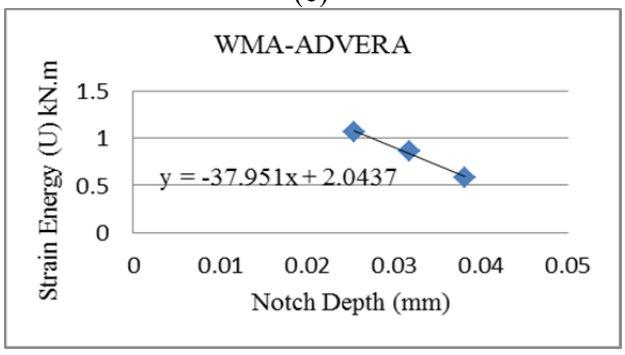


(g)

**FIGURE 11, Strain Energy Curves for Modified HMA Mixtures**
**a. PG64-10RAP b. PG64-28PM c. 710P4-AR d. AN-HMA e. AN-WMA f. MnROAD g. WMA-ADVERA**

**TABLE 4, SCB CHM Method Test Results ($J_c$)**

| Mix Type | Notch Size (mm) | U (kN.m) | CV | $J_c$ (lb/in) | $J_c$ (kN/m) | Rank |
|---|---|---|---|---|---|---|
| **PG64-10RAP (LIME)** | 25.40 | 1.246 | 3% | 7.9 | 0.662 | 7 |
| | 31.75 | 1.032 | 1% | | | |
| | 38.10 | 0.797 | 10% | | | |
| **PG64-28PM (LIME)** | 25.40 | 1.051 | 28% | 9.8 | 0.816 | 4 |
| | 31.75 | 0.749 | 18% | | | |
| | 38.10 | 0.498 | 26% | | | |
| **710P4-AR** | 25.40 | 1.543 | 11% | 13.6 | 1.132 | 2 |
| | 31.75 | 1.269 | 13% | | | |
| | 38.10 | 0.776 | 22% | | | |
| **AN-HMA** | 25.40 | 1.113 | 37% | 8.3 | 0.696 | 6 |
| | 31.75 | 0.810 | 15% | | | |
| | 38.10 | 0.642 | 21% | | | |
| **AN-WMA** | 25.40 | 1.155 | 17% | 10.4 | 0.866 | 3 |
| | 31.75 | 0.896 | 35% | | | |
| | 38.10 | 0.568 | 32% | | | |
| **MnROAD** | 25.40 | 1.325 | 29% | 14.4 | 1.198 | 1 |
| | 31.75 | 1.259 | 0% | | | |
| | 38.10 | 0.513 | 27% | | | |
| **WMA-ADVERA** | 25.40 | 1.069 | 4% | 8.5 | 0.711 | 5 |
| | 31.75 | 0.860 | 38% | | | |
| | 38.10 | 0.587 | 12% | | | |

**TABLE 5, SCB CHM Method Test Results ($K_{1c}$)**

| Mix Type | Notch Size (mm) | $K_{1c}$ (N/m$^2$) | CV | $K_{1c}$ (N/m$^2$) | Rank |
|---|---|---|---|---|---|
| **PG64-10RAP (LIME)** | 25.4 | 4.36 | 2% | 4.43 | 1 |
| | 31.75 | 4.99 | 16% | | |
| | 38.1 | 4.69 | 10% | | |
| **PG64-28PM (LIME)** | 25.4 | 3.18 | 23% | 2.88 | 4 |
| | 31.75 | 2.58 | 14% | | |
| | 38.1 | 2.29 | 16% | | |
| **710P4-AR** | 25.4 | 4.41 | 5% | 4.12 | 2 |
| | 31.75 | 5.16 | 17% | | |
| | 38.1 | 3.65 | 7% | | |
| **AN-HMA** | 25.4 | 3.87 | 22% | 3.62 | 3 |
| | 31.75 | 2.80 | 35% | | |
| | 38.1 | 2.65 | 28% | | |
| **AN-WMA** | 25.4 | 2.65 | 0% | 2.46 | 6 |
| | 31.75 | 2.90 | 15% | | |
| | 38.1 | 2.46 | 23% | | |
| **MnROAD** | 25.4 | 1.75 | 4% | 1.70 | 7 |
| | 31.75 | 1.79 | 1% | | |
| | 38.1 | 1.55 | 6% | | |
| **WMA-ADVERA** | 25.4 | 2.87 | 11% | 2.69 | 5 |
| | 31.75 | 3.08 | 18% | | |
| | 38.1 | 2.95 | 14% | | |

**TABLE 6a, ANOVA for SCB CHM, $J_c$ Values, 95.0% Confidence and TABLE 6b, Tukey Analysis on $J_c$, 95.0% Confidence**

| Source | DF | Seq SS | Adj SS | Adj MS | F | P |
|---|---|---|---|---|---|---|
| MixNom | 6 | 5.6E-01 | 5.6E-01 | 9.3E-02 | 4.39 | 0.037 |
| Error | 7 | 1.5E-01 | 1.5E-01 | 2.1E-02 | | |
| Total | 13 | 7.0E-01 | | | | |

**TABLE 6b, Tukey Analysis on $J_c$, 95.0% Confidence**

| Mixture | Mean*10^2 | Grouping |
|---|---|---|
| MnROAD | 1.2 | A |
| 710P4-AR | 1.1 | A |
| AN-WMA | 0.9 | A |
| PG64-28PM (LIME) | 0.8 | A |
| WMA-ADVERA | 0.7 | A |
| AN-HMA | 0.7 | A |
| PG64-10RAP (LIME) | 0.7 | A |

**TABLE 7a, ANOVA for SCB CHM, $J_c$ Values, 80.0% Confidence and TABLE 7b, Tukey Analysis on $J_c$, 80.0% Confidence**

| Source | DF | Seq SS | Adj SS | Adj MS | F | P |
|---|---|---|---|---|---|---|
| Mixture | 6 | 8.0E+05 | 8.0E+05 | 1.3E+05 | 4.39 | 0.037 |
| Error | 7 | 2.1E+05 | 2.1E+05 | 3.0E+04 | | |
| Total | 13 | 1.0E+06 | | | | |

**TABLE 7b, Tukey Analysis on $J_c$, 80.0% Confidence**

| Mixture | Mean*10^2 | Grouping |
|---|---|---|
| MnROAD | 1.2 | A |
| 710P4-AR | 1.1 | A |
| AN-WMA | 0.9 | AB |
| PG64-28PM (LIME) | 0.8 | AB |
| WMA-ADVERA | 0.7 | B |
| AN-HMA | 0.7 | B |
| PG64-10RAP (LIME) | 0.7 | B |

**TABLE 8a, ANOVA for SCB CHM, $K_{1c}$ Values, 95% Confidence and TABLE 8b, Tukey Analysis on $K_{1c}$, 95.0% Confidence**

| Source | DF | Seq SS | Adj SS | Adj MS | F | P |
|---|---|---|---|---|---|---|
| Mixture | 6 | 3.2E+01 | 3.2E+01 | 5.3E+00 | 22.62 | 0 |
| Error | 32 | 7.5E+00 | 7.5E+00 | 2.3E-01 | | |
| Total | 38 | 3.9E+01 | | | | |

**TABLE 8b, Tukey Analysis on $K_{1c}$, 95.0% Confidence**

| Mixture | Mean*10^2 | Grouping |
|---|---|---|
| PG64-10RAP (LIME) | 4.4 | A |
| 710P4-AR | 4.1 | A |
| AN-HMA | 3.6 | AB |
| PG64-28PM (LIME) | 2.8 | BC |
| WMA-ADVERA | 2.7 | BC |
| AN-WMA | 2.5 | CD |
| MnROAD | 1.7 | D |

## 8.2. Semi-Circular Bend (SCB) Test, Camera Method

A total of 18 SCB tests with camera method were performed on six mixtures (PG64-10, PG64-28, 710P4-AR, AN-HMA, AN-WMA and WMA-ADVERA) with three notch-depths (1, 1.25 and 1.5 inch).

Like Figure 10, the load-displacement curves for three notch depths of HMA mixtures was drawn. The maximum load ($F_{max}$) was recorded and the area under the load displacement curve was used to determine the strain energy (U). The calculated strain energy for each notch was used to determine the critical strain energy $J_c$, as shown in Figure 11. By dividing the slope of the linear fitting line to the spaceman's thickness the $J_c$ value can be calculated. The calculated peak load and the dissipated energy for each SCB test were used to determine the critical $K_{1c}$ and $J_c$ values, Equations 1 and 2.

The SCB camera method, $J_c$ and $K_{1c}$ values for each AC mixture are presented in Table 9. The table presents the dissipated energy (U), the critical value of the J-integral ($J_c$), and the ranking of the mixtures based on the $J_c$ and $K_{1c}$ parameters. The value of $J_c$ ranged from 0.226 to 1.559 kN.m. The value of $K_{1c}$ ranged from 2.7825 to5.2805 N /$m^2$.

As with the SCB cross-head movement method, analysis of variance (ANOVA) is used in this method in order to have a better comparison of mixtures ranking. Using ANOVA, the P-value is used to determine the significance of the model. Typically P is compared to an alpha value of 0.05. A P-value that is lower than alpha indicates that the model is significant. The Tukey analysis, which is a part of ANOVA, was used to examine the difference in the groups with different rankings.

In order to categorize $J_c$ and $K_{1c}$ values, Tukey analysis with 95% degree of confidence was performed on the data. Test results ranking ($J_c$ and $K_{1c}$) as well as ANOVA ranking for the mixtures are provided in Table 10.

**TABLE 9, SCB Camera Method Results ($J_c$) and ($K_{1c}$)**

| Mix Type | Notch (mm) | U (kN.m) | $J_c$ (kN/m) | Rank | $K_{1c}$ (N/m2) | Rank |
|---|---|---|---|---|---|---|
| PG64-10RAP | 25.4 | 0.5153 | 0.271 | 5 | 5.2805 | 1 |
| | 31.75 | 0.273 | | | | |
| | 38.1 | 0.3316 | | | | |
| PG64-28PM | 25.4 | 0.612 | 0.676 | 3 | 3.0774 | 4 |
| | 31.75 | 0.1872 | | | | |
| | 38.1 | 0.1535 | | | | |
| 710P4-AR | 25.4 | 0.9953 | 1.137 | 2 | 4.8487 | 2 |
| | 31.75 | 0.6943 | | | | |
| | 38.1 | 0.225 | | | | |
| AN-HMA | 25.4 | 0.369 | 0.226 | 6 | 2.7825 | 6 |
| | 31.75 | 0.2557 | | | | |
| | 38.1 | 0.216 | | | | |
| AN-WMA | 25.4 | 1.2261 | 1.559 | 1 | 2.9717 | 5 |
| | 31.75 | 0.4374 | | | | |
| | 38.1 | 0.17 | | | | |
| WMA-ADVERA | 25.4 | 0.3116 | 0.281 | 4 | 3.2553 | 3 |
| | 31.75 | 0.1434 | | | | |
| | 38.1 | 0.1213 | | | | |

**TABLE 10, SCB Camera Method Ranking ($J_c$) and ($K_{1c}$)**

| Mix Type | $J_c$ Camera | $J_c$ Camera | $K_{1c}$ Camera | $K_{1c}$ Camera |
|---|---|---|---|---|
| PG64-10RAP | A | 5 | A | 1 |
| PG64-28PM | A B | 3 | A | 4 |
| 710P4-AR | B C | 2 | B | 2 |
| AN-HMA | C | 6 | B | 6 |
| AN-WMA | C | 1 | B | 5 |
| WMA-ADVERA | C | 4 | B | 3 |

## 8.3. Beam Fatigue Test (BFT)

A total of 21 BFT's were performed: Seven mixtures (PG64-10, PG64-28, 710P4-AR, AN-HMA, AN-WMA, MnROAD and WMA-ADVERA) and three replicates each. The test was performed at 20 °C and strain level of 400 micro-strains. The dissipated energy, number of cycles to failure (Nf), initial stiffness, average ratio of dissipated energy (RDEC) and plateau value (PV) were determined for all conducted BFT.

Figure 12 presents dissipated energy verses number of cycles to failure and the fitting curve was determined. The fitting curve parameter, "k", was used in PV calculation, Equation 8.

Tables (11), (12) and (13) present initial stiffness, $N_f$, and PV values, respectively, for the conducted BFT. The tables present the average of three replicates for each mixture with the exception of 710P4-AR, for which BFT was conducted in two replicates. In order to compare the test results, the ranking for each test parameter was considered. Furthermore, to check the variability of the test results, coefficient of variation for the test results was calculated. In table 12 the results of the Nf parameter are presented. It can be seen that the CV values were extremely high for three mixtures (PG 64-10RAP, PG64-28PM, and AN-HMA). In order to reduce the coefficient of variation, it was decided to split the results into two scenarios beside the original results.

As can be seen in the tables, in order to reduce the CV, in the first scenario the higher values are eliminated and in the second one, the lower values are eliminated. The difference between the two modified groups is the way that each eliminates outlier test results. As can be seen, in both scenarios, an effort is made to reduce the coefficient of variation to reduce the coefficient of variation. When the ranking of both scenarios are compared, it can be seen that the ranking did not changed significantly, except for AN-HMA mixture. Therefore, the analysis was continued based on the first scenario.

The ANOVA with 95% degree of confidence was also done on original BFT results. The initial stiffness, $N_f$ and PV results are presented in Tables (14a), (15a) and (16a), respectively. The analysis shows that these three parameters are significant, as the P-value is lower than 0.05. Tukey analysis with 95% confidence was performed to analyze initial stiffness, Nf and PV values, Tables (14b), (15b) and (16b), respectively. Tukey analysis indicates that original initial stiffness, PV and Nf values can be categorized in one, two, and three groups, respectively.

Another series of ANOVA was done on modified BFT results. The results for initial stiffness, $N_f$ and PV values with 95% degree of confidence are presented in Tables (17a), (19a) and (20a), and the results show that the P-value for all three parameters is lower than 0.05, which indicates their significance. Tables (17b), (19b) and (20b) present the Tukey analysis results for initial stiffness, Nf and PV values. Tables (19b) and (20b), categorize Nf and PV parameters in four and six groups, respectively. Table (18a) presents ANOVA for initial stiffness with a 60% degree of confidence. The reason that ANOVA was done with a 60% degree of confidence for this parameter is that the Tukey analysis with a 95% degree of confidence categorized initial stiffness values in one group, Table (17b). As the comparison needs more than one group, the analysis with a 60% degree of confidence was also provided, Table (18b). As a result, three groups were generated.

Tukey analysis results show that $N_f$ and PV parameter rankings in Tables (12) and (13) correlate well with those in Table (19b) and (20b). The Nf values, which ranked (1), (2), (3, 4, 5, 6) and (7) in Table (12) are categorized separately as A, B, BC and C in Table (19b). Similarly the PV ranking in Table (13) is correlated to that of Table (20b).

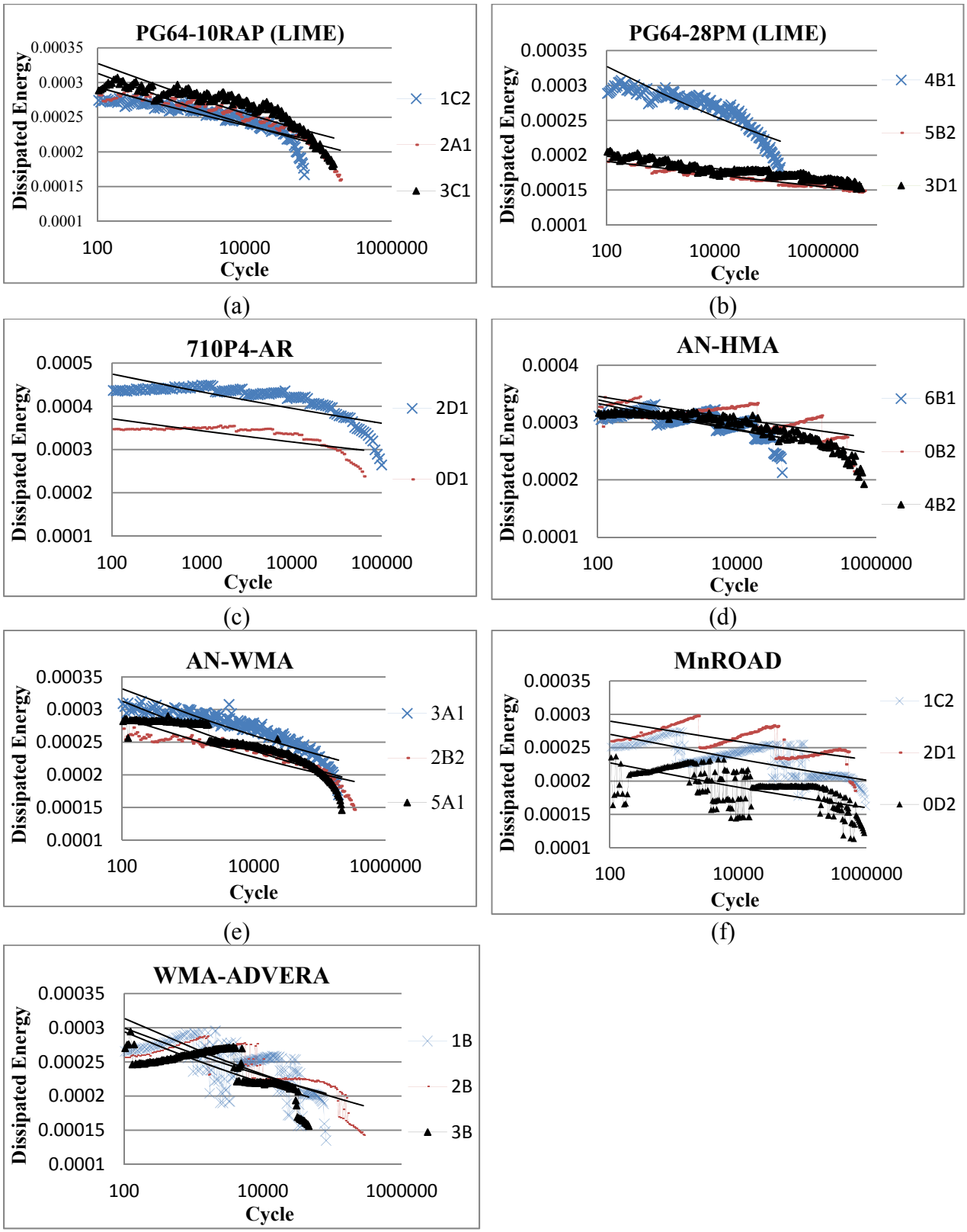


**FIGURE 12, Rate of Dissipated Energy at 400MH Strain Level a. PG64-10RAP b. PG64-28PM c. 710P4-AR d. AN-HMA e. AN-WMA f. MnROAD g. WMA-ADVERA**

**TABLE 11, BFT Results (Initial Stiffness)**

| Mix Type | Rep[a] | Original Test Results | | | Modified Test Results First scenario | | | Modified Test Results Second Scenario | | |
|---|---|---|---|---|---|---|---|---|---|---|
| | | Ini S[b] (MPA) | Ini S (MPA) | CV (%) | Ini S | Ini S M1 | Rank | Ini S | Ini S M2 | Rank |
| PG64-10RAP (LIME) | 1 | 5235 | 5423 | 10.00 | 5235 | 5235 | 5 | | 5516 | 3 |
| | 2 | 4983 | | | | | | 4983 | | |
| | 3 | 6050 | | | | | | 6050 | | |
| PG64-28PM (LIME) | 1 | 6050 | 3561 | 61.00 | 6050 | 6050 | 3 | | 2316 | 7 |
| | 2 | 2257 | | | | | | 2257 | | |
| | 3 | 2375 | | | | | | 2375 | | |
| 710P4-AR | 1 | 7280 | 6670 | 13.00 | 7280 | 6670 | 2 | 7280 | 6670 | 2 |
| | 2 | 6060 | | | 6060 | | | 6060 | | |
| AN-HMA | 1 | 5855 | 5441 | 11.00 | 5855 | 5855 | 4 | | 5234 | 4 |
| | 2 | 5744 | | | | | | 5744 | | |
| | 3 | 4723 | | | | | | 4723 | | |
| AN-WMA | 1 | 4852 | 4294 | 12.00 | 4852 | 4294 | 6 | 4852 | 4294 | 5 |
| | 2 | 4238 | | | 4238 | | | 4238 | | |
| | 3 | 3791 | | | 3791 | | | 3791 | | |
| MnROAD | 1 | 3525 | 3488 | 24.00 | 3525 | 3488 | 7 | 3525 | 3488 | 6 |
| | 2 | 4302 | | | 4302 | | | 4302 | | |
| | 3 | 2636 | | | 2636 | | | 2636 | | |
| WMA-ADVERA | 1 | 81751 | 136520 | 93.00 | 81751 | 136520 | 1 | 81751 | 136520 | 1 |
| | 2 | 281837 | | | 281837 | | | 281837 | | |
| | 3 | 45971 | | | 45971 | | | 45971 | | |

a. Rep = Replicate
b. Ini S= Initial Stiffness

**TABLE 12, BFT Results (Nf)**

| Mix Type | Rep | Original Test Results | | | Modified Test Results First Scenario | | | Modified Test Results Second Scenario | | |
|---|---|---|---|---|---|---|---|---|---|---|
| | | Nf | Nf | CV (%) | Nf | Nf M1 | Rank | Nf | Nf M2 | Rank |
| PG64-10RAP (LIME) | 1 | 64937 | 142526 | 49 | 64937 | 64937 | 5 | | 181321 | 5 |
| | 2 | 199525 | | | | | | 199525 | | |
| | 3 | 163116 | | | | | | 163116 | | |
| PG64-28PM (LIME) | 1 | 163116 | 3702985 | 83 | 163116 | 163116 | 3 | | 5472919 | 1 |
| | 2 | 5787618 | | | | | | 5787618 | | |
| | 3 | 5158220 | | | | | | 5158220 | | |
| 710P4-AR | 1 | 99999 | 83416 | 28 | 99999 | 83416 | 4 | 99999 | 83416 | 6 |
| | 2 | 66833 | | | 66833 | | | 66833 | | |
| AN-HMA | 1 | 44667 | 395386 | 81 | 44667 | 44667 | 6 | | 570746 | 3 |
| | 2 | 473150 | | | | | | 473150 | | |
| | 3 | 668342 | | | | | | 668342 | | |
| AN-WMA | 1 | 193864 | 248782 | 30 | 193864 | 248782 | 2 | 193864 | 248782 | 4 |
| | 2 | 334964 | | | 334964 | | | 334964 | | |
| | 3 | 217519 | | | 217519 | | | 217519 | | |
| MnROAD | 1 | 971626 | 846093 | 20 | 971626 | 846093 | 1 | 971626 | 846093 | 2 |
| | 2 | 649380 | | | 649380 | | | 649380 | | |
| | 3 | 917274 | | | 917274 | | | 917274 | | |
| WMA-ADVERA | 1 | 3757 | 3700 | 2 | 3757 | 3700 | 7 | 3757 | 3700 | 7 |
| | 2 | 3619 | | | 3619 | | | 3619 | | |
| | 3 | 3722 | | | 3722 | | | 3722 | | |

**TABLE 13, BFT Results (PV)**

| Mix Type | Rep | Original Test Results | | | Modified Test Results First Scenario | | | Modified Test Results Second Scenario | | |
|---|---|---|---|---|---|---|---|---|---|---|
| | | PV *E09 | Pv Ave *E09 | CV | PV *E09 | PV M1 *E09 | Rank | PV *E09 | PV M2 *E09 | Rank |
| PG64-10RAP (LIME) | 1 | 693 | 438 | 0.51 | 693 | 693 | 5 | | 311 | 5 |
| | 2 | 291 | | | | | | 291 | | |
| | 3 | 331 | | | | | | 331 | | |
| PG64-28PM (LIME) | 1 | 331 | 113 | 1.67 | 331 | 331 | 3 | | 4 | 1 |
| | 2 | 4 | | | | | | 4 | | |
| | 3 | 4 | | | | | | 4 | | |
| 710P4-AR | 1 | 400 | 454 | 0.17 | 400 | 454 | 4 | 400 | 454 | 6 |
| | 2 | 509 | | | 509 | | | 509 | | |
| AN-HMA | 1 | 739 | 283 | 1.4 | 739 | 739 | 6 | | 54 | 3 |
| | 2 | 55 | | | | | | 55 | | |
| | 3 | 54 | | | | | | 54 | | |
| AN-WMA | 1 | 273 | 234 | 0.3 | 273 | 234 | 2 | 273 | 234 | 4 |
| | 2 | 152 | | | 152 | | | 152 | | |
| | 3 | 276 | | | 276 | | | 276 | | |
| MnROAD | 1 | 33 | 37 | 0.11 | 33 | 37 | 1 | 33 | 37 | 2 |
| | 2 | 37 | | | 37 | | | 37 | | |
| | 3 | 41 | | | 41 | | | 41 | | |
| WMA-ADVERA | 1 | 15438 | 16956 | 0.08 | 15438 | 16956 | 7 | 15438 | 16956 | 7 |
| | 2 | 18236 | | | 18236 | | | 18236 | | |
| | 3 | 17193 | | | 17193 | | | 17193 | | |

**TABLE 14a, ANOVA for BFT Original Initial Stiffness Values, 95.0% Confidence and TABLE 14b, Tukey Analysis, Original Initial Stiffness Values**

| Source | DF | Seq SS | Adj SS | Adj MS | F | P |
|---|---|---|---|---|---|---|
| Mixture | 6 | 4.4E+10 | 4.4E+10 | 7.4E+09 | 2.97 | 0.047 |
| Error | 13 | 3.2E+10 | 3.2E+10 | 2.5E+09 | | |
| Total | 19 | 7.7E+10 | | | | |

**TABLE 14b, Tukey Analysis, Original Initial Stiffness Values**

| Mixture | Mean | Group |
|---|---|---|
| WMA-ADVERA | 136520 | A |
| 710P4-AR | 6670 | A |
| AN-HMA | 5441 | A |
| PG64-10RAP | 5423 | A |
| AN-WMA | 4294 | A |
| PG64-28PM | 3561 | A |
| MnROAD | 3488 | A |

**TABLE 15a, ANOVA for BFT Original Nf Values, 95.0% Confidence and TABLE 15b, Tukey Analysis, Original Nf values**

| Source | DF | Seq SS | Adj SS | Adj MS | F | P |
|---|---|---|---|---|---|---|
| Mixture | 6 | 3.1E+13 | 3.1E+13 | 5.2E+12 | 3.47 | 0.028 |
| Error | 13 | 1.9E+13 | 1.9E+13 | 1.5E+12 | | |
| Total | 19 | 5.0E+13 | | | | |

**TABLE 15b, Tukey Analysis, Original Nf values**

| Mixture | Mean | Group |
|---|---|---|
| PG64-28PM | 3702985 | A |
| MnROAD | 846093 | AB |
| AN-HMA | 395386 | AB |
| AN-WMA | 248782 | B |
| PG64-10RAP | 142526 | B |
| 710P4-AR | 83416 | B |
| WMA-ADVERA | 3700 | B |

**TABLE 16a, ANOVA for BFT Original PV Values, 95.0% Confidence and TABLE 16b, Tukey Analysis, Original PV values**

| Source | DF | Seq SS | Adj SS | Adj MS | F | P |
|---|---|---|---|---|---|---|
| Mixture | 6 | 7.1E+08 | 7.1E+08 | 1.2E+08 | 346.71 | 0 |
| Error | 13 | 4.4E+06 | 4.4E+06 | 3.4E+05 | | |
| Total | 19 | 7.1E+08 | | | | |

**TABLE 16b, Tukey Analysis, Original PV values**

| Mixture | Mean | Group |
|---|---|---|
| MnROAD | 37.1 | A |
| AN-WMA | 233.8 | A |
| AN-HMA | 282.5 | A |
| PG64-28PM | 367 | A |
| PG64-10RAP | 438.2 | A |
| 710P4-AR | 454.4 | A |
| WMA-ADVERA | 16955.7 | B |

**TABLE 17 a, ANOVA for BFT, Modified Initial Stiffness, 95.0% Confidence and TABLE 17b, Tukey Analysis, Modified Initial Stiffness Values**

| Source | DF | Seq SS | Adj SS | Adj MS | F | P |
|---|---|---|---|---|---|---|
| Mixture | 6 | 4.1E+10 | 4.1E+10 | 6.8E+09 | 1.47 | 0.31 |
| Error | 7 | 3.2E+10 | 3.2E+10 | 4.6E+09 | | |
| Total | 13 | 7.3E+10 | | | | |

**TABLE 17b, Tukey Analysis, Modified Initial Stiffness Values**

| Mixture | Mean | Grouping |
|---|---|---|
| WMA-ADVERA | 136520 | A |
| 710P4-AR | 6670 | A |
| PG64-28PM (LIME) | 6050 | A |
| AN-HMA | 5855 | A |
| PG64-10RAP (LIME) | 5235 | A |
| AN-WMA | 4294 | A |
| MnROAD | 3488 | A |

**TABLE 18a, ANOVA for BFT, Modified Initial Stiffness, 60.0% Confidence and TABLE 18b, Tukey Analysis, Modified Initial Stiffness Values**

| Source | DF | Seq SS | Adj SS | Adj MS | F | P |
|---|---|---|---|---|---|---|
| Mixture | 6 | 4.1E+10 | 4.1E+10 | 6.8E+09 | 1.47 | 0.31 |
| Error | 7 | 3.2E+10 | 3.2E+10 | 4.6E+09 | | |
| Total | 13 | 7.3E+10 | | | | |

**TABLE 18b, Tukey Analysis, Modified Initial Stiffness Values**

| Mixture | Mean | Grouping |
|---|---|---|
| WMA-ADVERA | 136519.7 | A |
| 710P4-AR | 6670.2 | AB |
| PG64-28PM (LIME) | 6049.9 | AB |
| AN-HMA | 5854.5 | AB |
| PG64-10RAP (LIME) | 5234.9 | AB |
| AN-WMA | 4293.7 | B |
| MnROAD | 3487.5 | B |

**TABLE 19a, ANOVA for BFT, Modified Nf, 95.0% Confidence and TABLE 19b, Tukey Analysis, Modified Nf Values**

| Source | DF | Seq SS | Adj SS | Adj MS | F | P |
|---|---|---|---|---|---|---|
| Mixture | 6 | 1.4E+12 | 1.4E+12 | 2.3E+11 | 22.58 | 0 |
| Error | 7 | 7.1E+10 | 7.1E+10 | 1.0E+10 | | |
| Total | 13 | 1.5E+12 | | | | |

**TABLE 19b, Tukey Analysis, Modified Nf Values**

| Mixture | Mean | Grouping |
|---|---|---|
| MnROAD | 846093.3 | A |
| AN-WMA | 248782.3 | B |
| PG64-28PM (LIME) | 163116 | BC |
| 710P4-AR | 83416 | BC |
| PG64-10RAP (LIME) | 64937 | BC |
| AN-HMA | 44667 | BC |
| WMA-ADVERA | 3699.5 | C |

**TABLE 20a, ANOVA for Modified BFT PV, 95.0% Confidence and TABLE 20b, Tukey Analysis, Modified PV Values**

| Source | DF | Seq SS | Adj SS | Adj MS | F | P |
|---|---|---|---|---|---|---|
| Mixture | 6 | 6.1E+05 | 6.1E+05 | 1.2E+05 | 38.48 | 0.001 |
| Error | 7 | 1.6E+04 | 1.6E+04 | 3.2E+03 | | |
| Total | 13 | 6.3E+05 | | | | |

**TABLE 20b, Tukey Analysis, Modified PV Values**

| Mixture | Mean *10^9 | Grouping |
|---|---|---|
| MnROAD | 37.1 | A |
| AN-WMA | 233.8 | B |
| PG64-28PM (LIME) | 331.1 | BC |
| 710P4-AR | 454.4 | CD |
| PG64-10RAP (LIME) | 693 | D |
| AN-HMA | 738.8 | D |
| WMA-ADVERA | 16955.7 | E |

# 9. Test Results Comparison

## 9.1. Comparison between SCB (Cross-Head Movement) and BFT

SCB test and BFT parameters ranking are provided in Table (21). Initial stiffness did not have good correlations with the other BFT parameters nor with the SCB parameters. This was expected, as it is consistent with previous studies that showed that the initial stiffness is not a good indicator of fracture properties of AC mixtures.

The ranking of first-modified $N_f$ and PV from the BFT is identical for test results. Based on the Tables 21 and 22, there is good relation between $J_c$ and $N_f$ and PV. Tukey analysis of $J_c$ grouped the PG64-10RAP (LIME), AN-HMA and WMA-ADVERA mixtures in the lowest grouping (B) and ranked (7, 6, and 5) respectively. Similarly the BFT $N_f$ grouped these mixtures in the lowest groups (BC, BC, and A) and they ranked (5, 6, and 7).

ANOVA was used to compare BFT and SCB test results. Table (22) shows the direct results from Tukey analysis, which categorized mixtures based on BFT and SCB test parameters. In order to better compare the Tukey analysis results, a constant scale was needed for the sake of demonstration of the results on a figure. Therefore, it was decided to convert the results from alphabetical to numerical formatting with a constant scale. A scale of four was chosen to convert the results. The converted results of the SCB test data as well as the BFT data is presented in Table (23).

The converted test results from the BFT and SCB test are used to correlate the parameters of these two tests. Figure (13) presents the correlation between the BFT and SCB test results. In this figure $J_c$ and $K_{1c}$ from the SCB test are plotted against PV and $N_f$ values from BFT. Figure (13a) and (13b) shows that there is a good correlation between the $N_f$ and PV with the $J_c$ values.

Figure (14) provides correlation between another SCB test parameter ($K_{1c}$), and BFT parameters ($N_f$ and PV). The correlation shows that the $K_{1c}$ have no correlation with the $N_f$ and PV, and that this correlation is almost the reverse of the previous one. This might be due to the fact that $K_{1c}$ is calculated based on the peak load without consideration of the deformation.

**TABLE 21, Specimens Ranking Comparison**

| Mix Type | Ini S | Ini S M1 | Ini S M2 | Nf | Nf M1 | Nf M2 | PV | PV M1 | PV M2 | Jc | Jc M | $K_{1c}$ | $K_{1c}$ M |
|---|---|---|---|---|---|---|---|---|---|---|---|---|---|
| **PG64-10RAP (LIME)** | 4 | 5 | 3 | 5 | 5 | 5 | 5 | 5 | 5 | 5 | 7 | 1 | 1 |
| **PG64-28PM (LIME)** | 6 | 3 | 7 | 1 | 3 | 1 | 2 | 3 | 1 | 6 | 4 | 4 | 4 |
| **710P4-AR** | 2 | 2 | 2 | 6 | 4 | 6 | 6 | 4 | 6 | 1 | 2 | 2 | 2 |
| **AN-HMA** | 3 | 4 | 4 | 3 | 6 | 3 | 4 | 6 | 3 | 7 | 6 | 3 | 3 |
| **AN-WMA** | 5 | 6 | 5 | 4 | 2 | 4 | 3 | 2 | 4 | 2 | 3 | 6 | 6 |
| **MnROAD** | 7 | 7 | 6 | 2 | 1 | 2 | 1 | 1 | 2 | 3 | 1 | 7 | 7 |
| **WMA-ADVERA** | 1 | 1 | 1 | 7 | 7 | 7 | 7 | 7 | 7 | 4 | 5 | 5 | 5 |

**TABLE 22, ANOVA for Modified Test Results Ranking**

| Mix Type | Nf M1 95% | PV M1 95% | $J_c$ M 80% | $K_{1c}$ 95% |
|---|---|---|---|---|
| **PG64-10RAP** | BC | D | B | A |
| **PG64-28PM** | BC | BC | AB | BC |
| **710P4-AR** | BC | CD | A | A |
| **AN-HMA** | BC | D | B | AB |
| **AN-WMA** | B | B | AB | CD |
| **MnROAD** | A | A | A | D |
| **WMA-ADVERA** | C | E | B | BC |

**TABLE 23, ANOVA for Modified Test Results Ranking**

| Mix Type | Nf M1 95% | PV M1 95% | $J_c$ M 80% | $K_{1c}$ 95% |
|---|---|---|---|---|
| **PG64-10RAP** | 3.00 | 3.33 | 4.00 | 1.00 |
| **PG64-28PM** | 3.00 | 2.00 | 2.67 | 2.40 |
| **710P4-AR** | 3.00 | 2.67 | 1.00 | 1.00 |
| **AN-HMA** | 3.00 | 3.33 | 4.00 | 1.60 |
| **AN-WMA** | 2.00 | 1.33 | 2.67 | 3.20 |
| **MnROAD** | 1.00 | 1.00 | 1.00 | 4.00 |
| **WMA-ADVERA** | 4.00 | 4.00 | 4.00 | 2.40 |

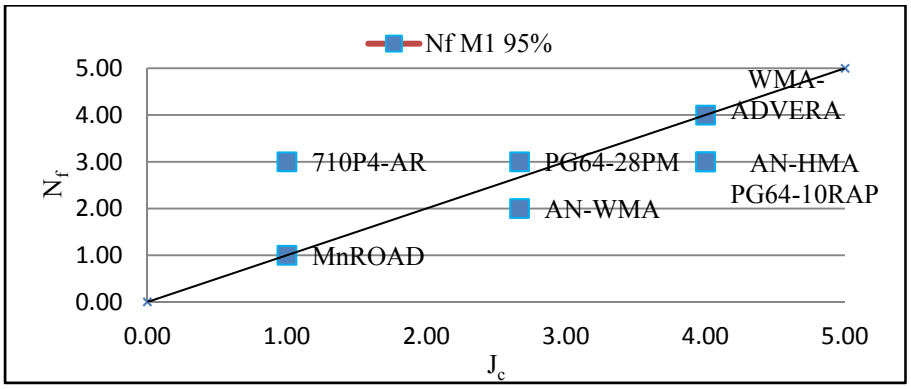


(a)

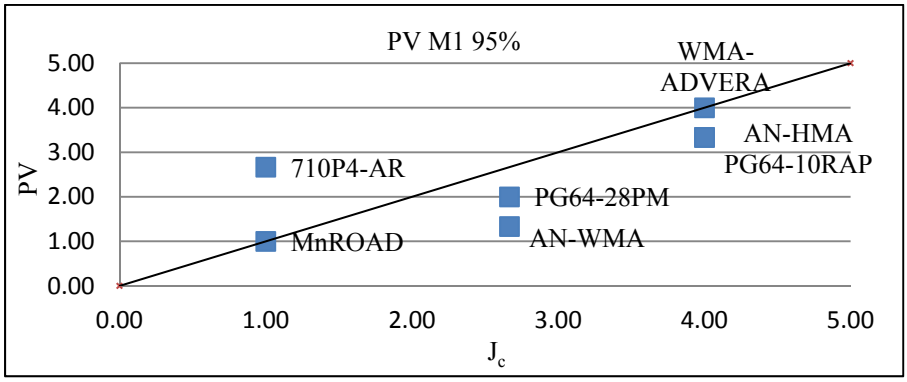


(b)

**FIGURE 13, BFT and SCB Test Results Correlation (a).Nf–$J_c$ (b).PV-$J_c$**

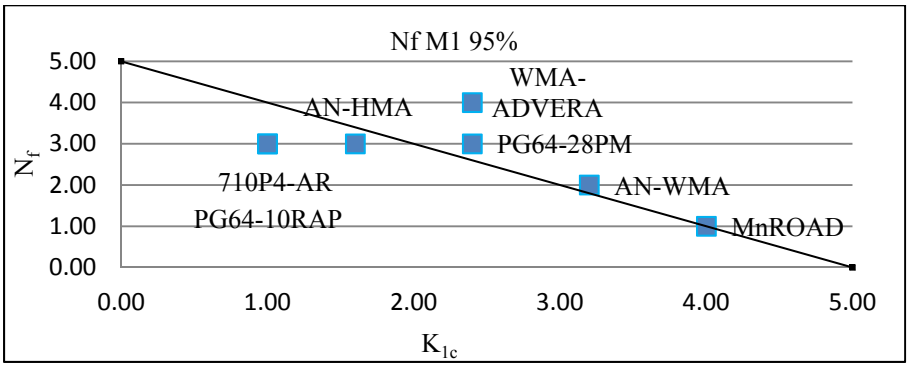


(a)

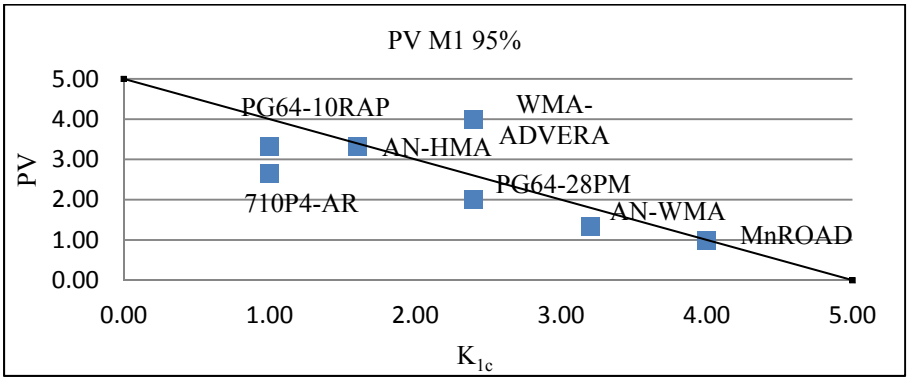


(b)

**FIGURE 14, BFT and Modified SCB Test Results Correlation (a).Nf–$K_{1c}$ (b).PV-$K_{1c}$**

## 9.2. Comparison between SCB Cross-Head Movement and Camera Methods

SCB test parameters ranking for both cross-head movement method (CHM) and camera method are provided in table (24). The table shows that there is a good correlation between parameters in both test methods; in addition, for further exploration of the test results, ANOVA was used to compare the test results.

Table (25) shows the direct results from Tukey analysis, which categorized mixtures based on SCB test parameters. In order to better compare the Tukey analysis results, a constant scale was needed. Therefore, it was decided to convert the results from alphabetical to numerical formatting using a constant scale. A scale of 4 was chosen to convert the results. The converted results of the SCB test data are also presented in Table (25).

The converted test results are used to correlate the parameters of these two test methods. Figure (15) presents the correlation between two SCB test result methods. In this figure $J_c$ and $K_{1c}$ from cross-head movement method is plotted against $J_c$ and $K_{1c}$ from the camera method. Figure (15a) shows that there is a linear correlation between the $J_c$ in the cross-head movement method and the camera method. Also, in Figure (15b) a linear correlation between $K_{1c}$ in the cross-head movement and camera methods is shown.

**TABLE 24, Specimens Ranking Comparison**

| Mix Type | $J_c$ Camera | $J_c$ CHM | $K_{1c}$ Camera | $K_{1c}$ CHM |
|---|---|---|---|---|
| PG64-10RAP | 5 | 6 | 1 | 1 |
| PG64-28PM | 3 | 3 | 4 | 4 |
| 710P4-AR | 2 | 1 | 2 | 2 |
| AN-HMA | 6 | 5 | 6 | 3 |
| AN-WMA | 1 | 2 | 5 | 6 |
| WMA-ADVERA | 4 | 4 | 3 | 5 |

**TABLE 25, ANOVA for Test Results Ranking**

| Mix Type | $J_c$ Camera | | $J_c$ CHM | | $K_{1c}$ Camera | | $K_{1c}$ CHM | |
|---|---|---|---|---|---|---|---|---|
| PG64-10RAP | A | 4.00 | A | 4.00 | A | 1.00 | A | 1.00 |
| PG64-28PM | A B | 3.00 | AB | 2.67 | A | 4.00 | A | 3.00 |
| 710P4-AR | B C | 2.00 | AB | 1.33 | B | 1.00 | AB | 1.00 |
| AN-HMA | C | 4.00 | B | 4.00 | B | 4.00 | BC | 2.00 |
| AN-WMA | C | 1.00 | B | 2.67 | B | 4.00 | BC | 4.00 |
| WMA-ADVERA | C | 4.00 | B | 4.00 | B | 4.00 | CD | 3.00 |

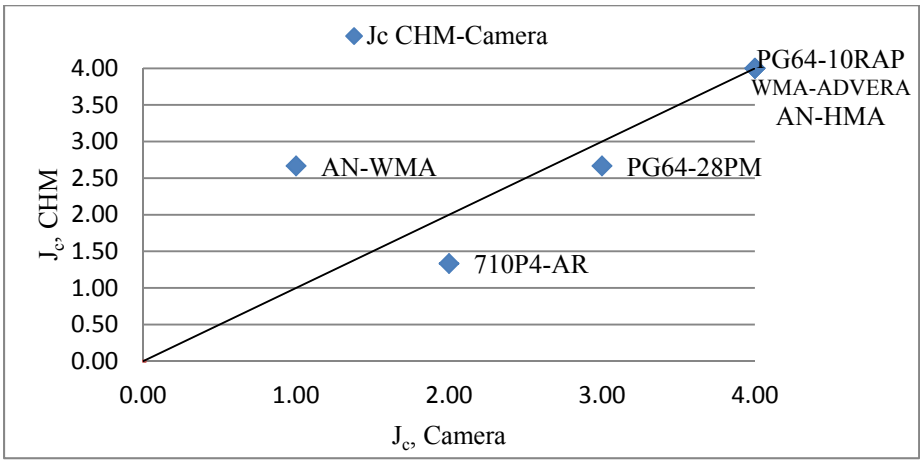


(a)

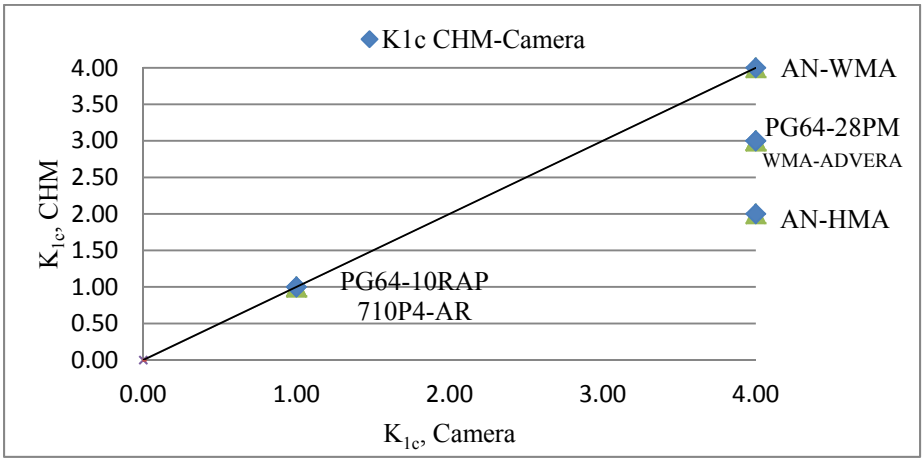


(b)

**FIGURE 15, SCB Cross-Head Movement and Camera Methods Test Results Correlation (a). $J_c$ (b). $K_{1c}$**

## 10.Modeling and Experimental Measurements

XFEM is a mesh independent finite element fracture modeling approach in which the FE mesh is generated independent of the crack, and the crack path and location are not specified. XFEM was introduced by Belytschko and Black [20] based on the partition of unity method of Babuska and Melenk [21]. The motivation behind the development of this approach was to allow finite element modeling of fracture that is independent of the mesh. The major advantages of this approach are the mesh is generated independent of the crack, and the crack path and location do not have to be specified. XFEM extends the piecewise polynomial function space of conventional finite element methods with extra functions. The extra functions enrich the solution space and hence such functions are called "enrichment functions." XFEM fracture modeling requires two enrichment functions, a Heaviside function to represent the displacement jump across crack face, and a crack tip asymptotic function to model singularity. The displacement interpolation function is as follows:

$$u^h(x) = \sum_{I\in N} N_I(x)[u_I + H(x)a_I + \sum_{\alpha=1}^{4} F_\alpha(x)b_I^\alpha] \quad [9]$$

where

$u_I$: nodal degree of freedom for conventional shape function $N_I$

H(x): Heaviside distribution,

$a_I$: nodal enriched degree of freedom (jump discontinuity),

Fα(x): crack tip asymptotic function

$b_I^\alpha$: Nodal degree of freedom for crack tip enrichment

In this equation, "$H(x)a_I$" is the Heaviside enrichment term in which $I \in N_\nabla$, and $N_\nabla$ is the set of nodes belonging to elements cut by a crack, while $\sum_{\alpha=1}^{4} F_\alpha(x)b_I^\alpha$ is crack tip enrichment term in which $I \in N_\Delta$, and $N_\Delta$ is the set of nodes belonging to the element's containing crack tip. The Heaviside function accounts for displacement jump across the crack and is defined as follow:

$$H(x) = \begin{cases} 1, & if\ (x - x^*).n \geq 0 \\ -1, & otherwise \end{cases} \quad [10]$$

where x is an integration point, x* is the closest point to x on the crack face and n is the unit normal to x*. Crack tip enrichment is defined in Equation 6 below:

$$[F_\alpha(x), \alpha = 1-4] = \left[\sqrt{r}\sin\frac{\theta}{2}, \sqrt{r}\cos\frac{\theta}{2}, \sqrt{r}\sin\frac{\theta}{2}\sin\theta, \sqrt{r}\sin\theta\cos\frac{\theta}{2}\right] \quad [11]$$

The purpose of this function is to account for crack tip singularity and it is based on the displacement field function for sharp cracks in an isotropic linear elastic material. However, crack tip enrichment is only required, and hence implemented, for stationary cracks only. For propagating cracks, a phantom node approach is implemented, and in this approach the discontinuous element with Heaviside enrichment is treated as a single element with real and phantom nodes that split into two parts. This method was introduced by Song et al [22] based on Hansbo and Hansbo's [23] formulation of a superimposed element. XFEM employs a "level set" method to locate cracks. A level set of a real-valued function is the set of all points at which the function attains a specified value. For example, the zero-valued level set of "*$f(x,y) = x^2 + y^2 - 25$*" is a circle of radius 5 centered at the origin. This is a popular technique that is usually used in interface tracking problems. A crack is completely defined with two functions φ and Ψ, with the level set φ = 0 representing the crack face, and the intersection of φ=0 and Ψ=0 representing the crack front. The two functions are defined by nodal values whose coordinates are determined

by the usual FE shape functions. Also, the functions are only evaluated for nodes that belong to elements cut by the crack. The ability of XFEM to predict fracture behavior with infrastructure materials was studied by Ng and Dai [24] and it was shown that XFEM is capable of predicting fracture for both homogeneous and heterogeneous infrastructure materials, including asphalt mixtures.

The CZM concept was introduced by Dugdale [25] for ductile materials, and serves as a computational method to model the fracture process though crack propagation. CZM is based on the assumption that a cohesive zone exists in the front crack tip which resists crack propagation (i.e. traction separation at a surface). CZM resistance to traction separation is explained in Figure 16, and is known as "traction-separation law." This figure defines a bilinear relationship between applied force and relative displacement through three main zones: 1) the pre-damage initiation zone which is dependent on the mechanical response of the material, when N is the peak strength, $\delta_{in}$ is the relative displacement at damage initiation point, and K is the stiffness in the elastic region, 2) the damage evolution zone from $\delta_{in}$ to $\delta_{fail}$, and 3) the crack propagation zone, once the crack propagation criterion is achieved ($\delta_{fail}$) then the crack will propagate. The area under the traction-displacement curve is the fracture energy of the material. Several researchers successfully used CZM to predict fracture in asphalt mixtures using SCB [26, 27, and 28].

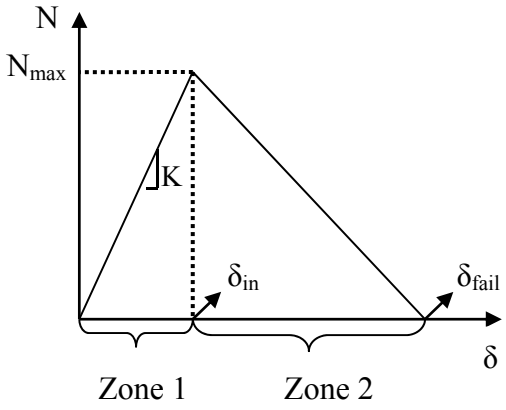


**FIGURE 16, Bilinear Traction-Separation Law Components**

## 10.1. XFEM-CZM Coupled Model

The commercially available software ABAQUS was used for FE modeling of the SCB test. The model geometry corresponds to the laboratory prepared SCB samples; dimensions of the model, location of the roller supports, and monotonic loading are also consistent with the lab experiment as previously described. The free medial axis quadratic elements meshing algorithm was used to generate model. Figure 17 illustrates the model for notch depths of 25.4, 31.8, and 38.0 mm. The asphalt mixture is modeled in this paper as a bulk viscoelastic material; ABAQUS defines the viscoelastic behavior based on a Prony series expansion of the dimensionless relaxation modulus. The series can be defined in one of four ways: creep test data, relaxation test data, direct specification of Prony series parameters, or frequency-dependent experimental data. In this study, Prony series coefficients reported by Abu Al-Rub et al. [29] were used, which are based on fitting the series to a single creep recovery asphalt mix data, with the adopted coefficients corresponding to the test conducted at 20 $^{o}$C.

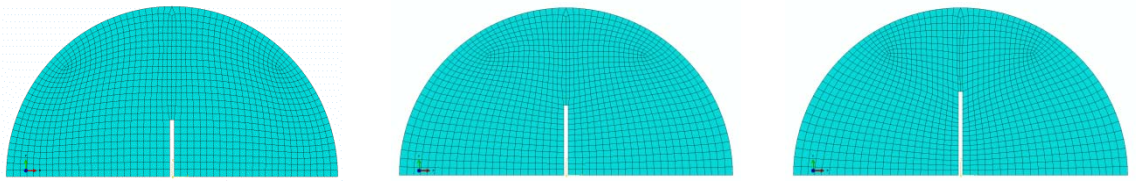

(a) (b) (c)

**Figure 17, ABAQUS FE Mesh: (a) 25.4 mm Notch, (b) 31.8 mm Notch, (c) 38.0 mm Notch**

XFEM was enabled by enriching all of the elements in the sample geometry. CZM was implemented to model damage. It's very important to mention that when CZM is implemented with traditional FE models (26, 27, and 28), ABAQUS requires a prior definition of crack location, and crack propagation is simulated by deleting elements as they crack. The coupling of XFEM with CZM used in this study allows for the damage initiation and crack propagation throughout the sample. No prior definition of crack location or direction is required, and a crack will initiate in any element that reaches the crack propagation criterion as described by bilinear traction-separation law.

The damage initiation criterion for bilinear traction-separation law in this study was based on the maximum principal stress (MAXPS). Equation 7 below defines the ratio R which is the ratio of maximum principal stress in an element to the maximum principal stress allowed, once the maximum principal stress in an element reaches a critical value (R=1) damage evolution will start.

$$R = \frac{\langle \sigma_n \rangle}{\sigma_{max}^{0}} \text{ and } \langle \sigma_n \rangle = \begin{cases} 0, & \sigma_n < 0 \\ \sigma_n, & \sigma_n > 0 \end{cases} \quad [12]$$

Damage evolution could be characterized by either specifying total fracture energy or the post-damage initiation relative displacement at failure, $\delta_{fail}$. The displacement criterion was selected for this study. It should be noted that the MAXPS criterion for damage initiation will only be effective in tension. Also, the crack plane is assumed to be perpendicular to the direction of the MAXPS and thus the crack plane is solution dependent. This also allows for change in crack plane and crack propagation direction, which better simulates the experimental results, as the crack propagation is not in actuality a straight perpendicular line.

The calibration process was achieved by iteratively changing the CZM parameters (MAXPS and $\delta_{fail}$) until the FE model results fit the experimental results. A similar approach was successfully used by other researchers (26 and 28). In order to better understand the effect of the

CZM parameters on the global fracture behavior of the SCB model, two parametric studies were conducted. First, initial MAXPS and $\delta_{fail}$ were randomly selected. In the first parametric study, MAXPS value was held constant while $\delta_{fail}$ was multiplied by the following factors: 1.5, 1.0, 0.7, and 0.5. In the second parametric study, $\delta_{fail}$ was held constant and MAXPS was multiplied by the following factors: 2.0, 1.0, 0.7, and 0.5. The simulation results are summarized in Figure 18. The variation of $\delta_{fail}$, as shown in Figure 18-a, mainly affects the location of the peak force and the post peak force behavior, and has a minor effect on the peak force value. On the other hand, changing MAXPS, Figure 18-b, mainly controls the peak force value and its location, and has a minor effect on the post-peak force behavior. Such parametric studies are extremely beneficial and usually provide a good starting point for the calibration – fitting process.

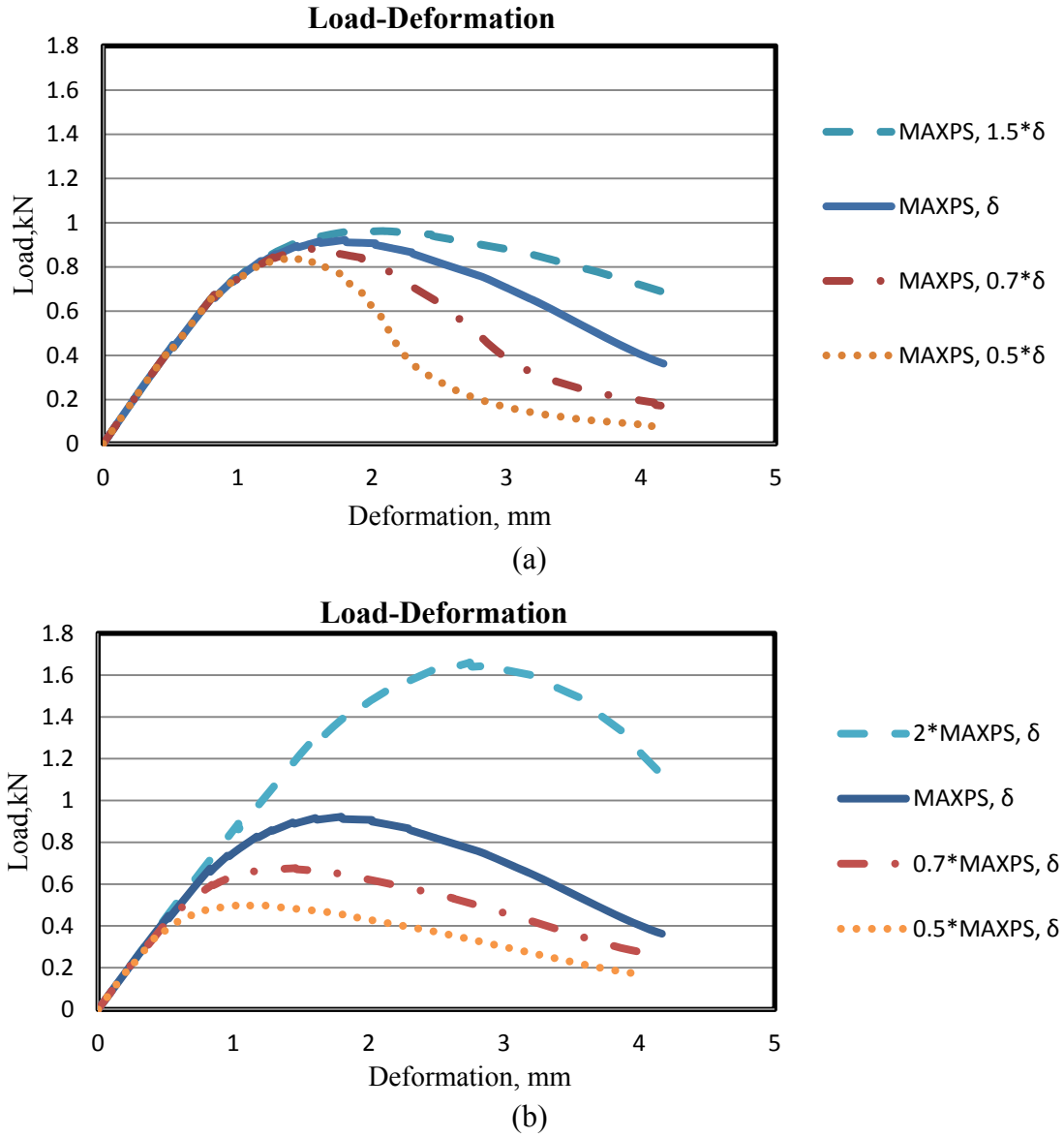


**Figure 18, CZM Parametric Study Results: (a) Variation of $\delta_{fail}$, (b) Variation of MAXPS.**

## 10.2. Modeling Results

Three asphalt mixtures were selected for FE modeling: 710P4-AR, AN-WMA, and WMA-Advera. For each of the mixtures, the experimental results for the 25.4 mm notch depth were used to calibrate the FE model. As described earlier, the calibration process consisted of changing MAXPS and $\delta_{fail}$ values until the FE simulation fit the experimental results. However, since the viscoelastic material properties were not available for all the mixes, the parameter K was changed such that the FE model fit the initial undamaged part of the test. Once the CZM parameters were calibrated to fit the SCB 25.4 mm notch depth experimental results, the parameters were then applied to the FE models developed for the 31.8 and 38.0 mm notch depth SCB geometries in order to verify if the experimental results can be predicted with FE simulations.

FE calibration and prediction compared to the experimental results data is illustrated in Figures 19, 20, and 21 for 710P4-AR, AN-WMA, and WMA-Advera mixtures, respectively. The figures clearly show that the FE calibration had a very good agreement with the experimental results, and it's obvious that the XFEM-CZM coupled model provides a suitable numerical tool to represent SCB testing. The results also illustrated that the model was successful in predicting the 31.8 and 38.0 mm notch depth SCB testing to a certain extent.

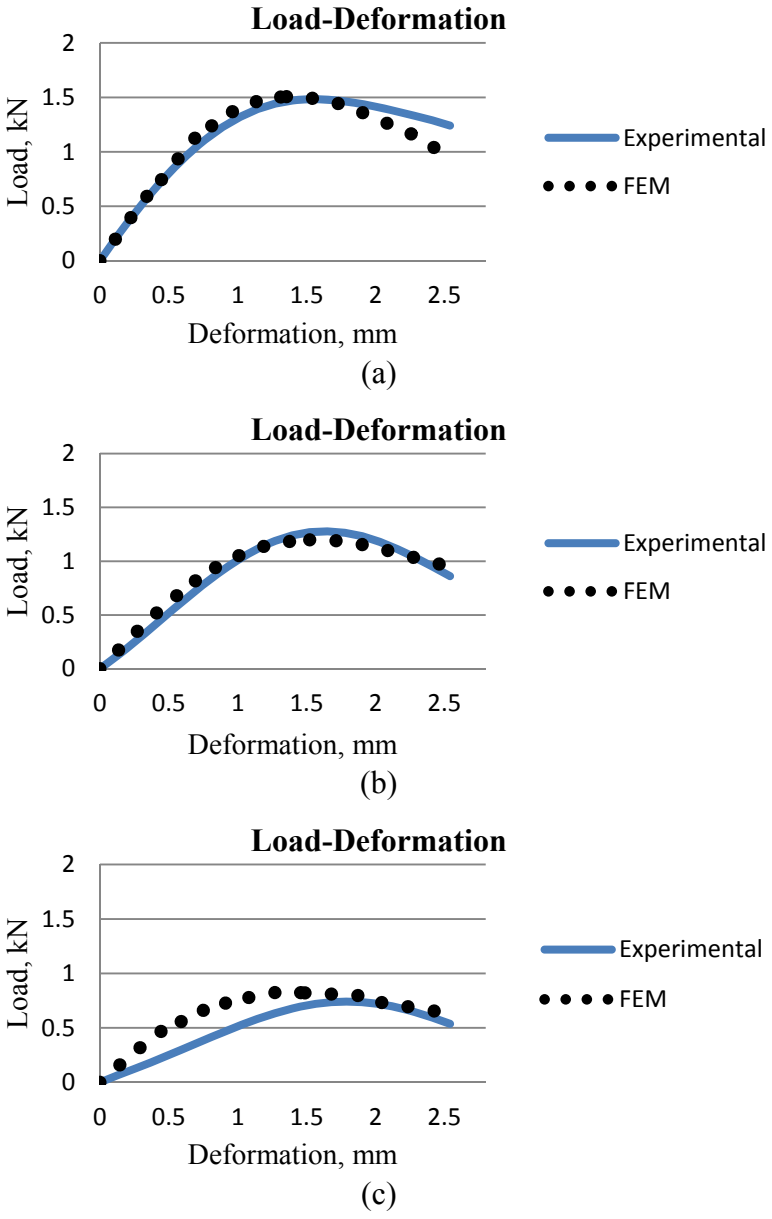


**Figure 19, 710P4-AR: (a) 25.4 mm Notch (Calibration), (b) 31.8 mm Notch (Prediction), (c) 38.0 mm Notch (Prediction)**

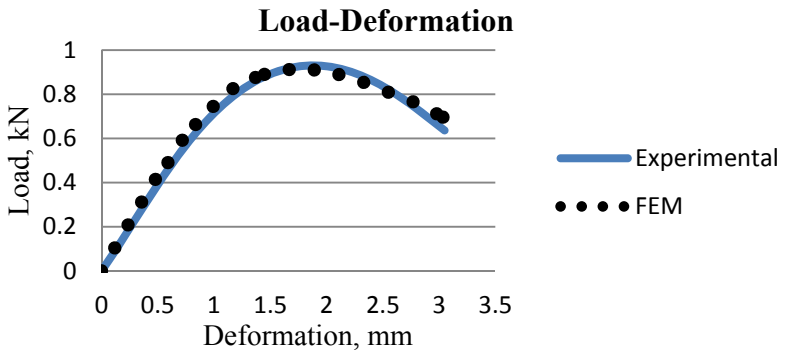


(a)

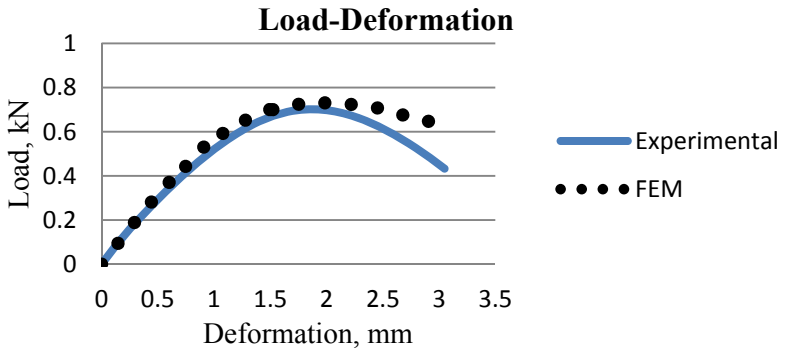


(b)

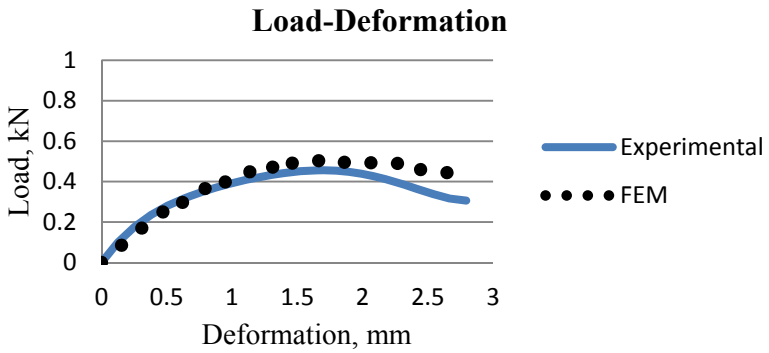


(c)

**Figure 20, AN-WMA: (a) 25.4 mm Notch (Calibration), (b) 31.8 mm Notch (Prediction), (c) 38.0 mm Notch (Prediction)**

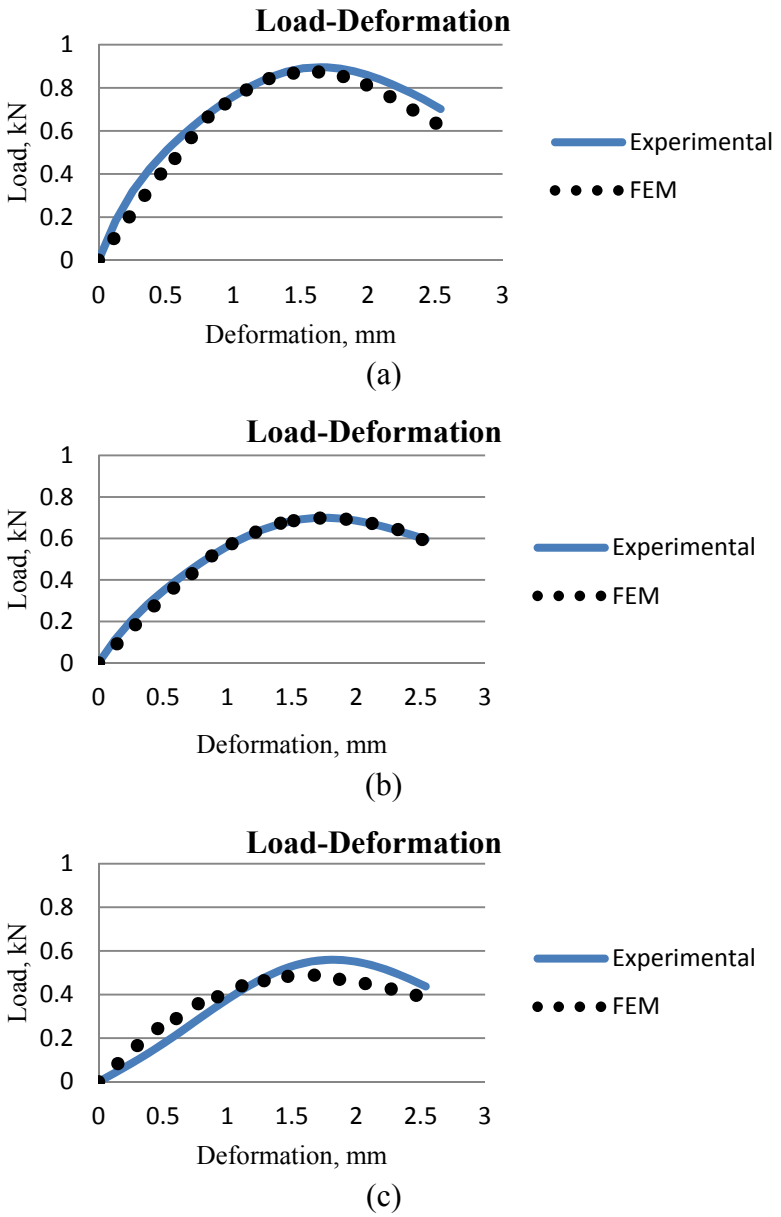


**Figure 21, WMA-A: (a) 25.4 mm Notch (Calibration), (b) 31.8 mm Notch (Prediction), (c) 38.0 mm Notch (Prediction)**

Crack propagation during the test was investigated using the FE model results. Figure 22 illustrates crack evolution in the SCB test as predicted by the FE model for the AN-WMA mixture with the 25.4 mm notch depth geometry. To study crack propagation, three points on the load-displacement curve were selected, A – crack initiation point, B – peak force point, and C – failure point (Figure 22-a). Crack propagation status at each loading point is shown in Figure b, c, and d for points A, B, and C, respectively. Due to stress concentration, a crack is initiated in the vicinity of the notch tip, when loading magnitude reaches point A the damage evolution criterion is reached for the element at the notch tip and the element will crack and split into two elements. The stress concentration will then transfer to the next element. This element will crack as the load increases, once the damage evolution criterion is satisfied. As the loading continues to increase, the crack will continue to propagate. As the crack propagates through, the material is enduring damage up until point B, at which point the damage level in the material is far enough along that less load is required for the crack to advance. As the displacement loading continues, the crack gradually progresses until the failure point is reached.

As described earlier, the crack plan is solution dependent, and it is perpendicular to the MAXPS. A vertical crack propagation line would indicate that the failure is completely attributed to tensile stresses. Figure 22 clearly indicates that the crack propagation occurs in the central strip of the specimen, and even though it's not perfectly vertical, it's obvious that the most significant component of the MAXPS is due to tensile stresses.

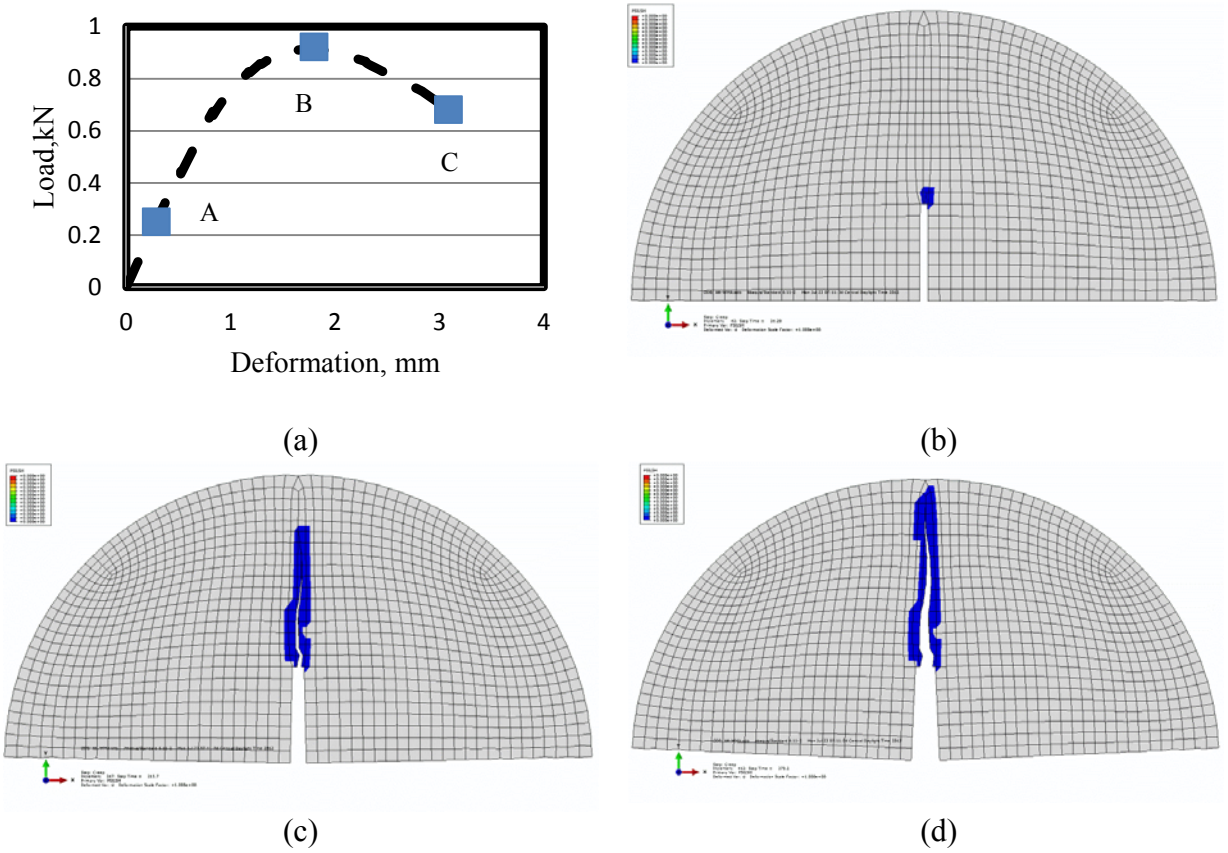


**Figure 22, Crack Propagation During SCB Test Predicted by FE Analysis**

# 11. Conclusion

The main objective of this study is to investigate the use of the SCB test as a quality QA/QC measure for field construction and comparison of fracture properties of HMA mixtures.

In SCB CHM method, $J_c$ and $K_{1c}$ values for (PG64-10RAP (LIME), PG64-28PM (LIME), 710P4-AR, AN-HMA, AN-WMA, MnROAD, WMA-ADVERA) mixtures were determined. BFT was performed on the same mixtures and initial stiffness, $N_f$ and PV for each mixture were determined. The following conclusions were drawn:

- The coefficient of variation (CV) ranged from 0 to 38% for $J_c$ and from 0 to 35% for $K_{1c}$.
- The coefficient of variation (CV) ranged from 10 to 93% for the initial stiffness, 2 to 83% for $N_f$, and 8 to 167% for PV.
- The SCB $J_c$ and BFT $N_f$ and PV indicated lower fracture properties for PG64-10RAP (LIME), AN-HMA and WMA-ADVERA mixtures than other mixtures.
- The BFT $N_f$ and PV achieved similar ranking.
- There is good correlation between $N_f$ and PV with $J_c$, and poor correlation between initial stiffness with $J_c$, $N_f$ and PV. This has indicated that the initial stiffness is not a good representative for fracture properties of AC while $J_c$, $N_f$ and PV are better indicators.
- The results of this study indicate that the SCB test has a great potential as a QA/QC test of fracture properties of asphalt mixtures.

In SCB test for both the Camera and CHM methods, $J_c$ and $K_{1c}$ values for (PG64-10RAP (LIME), PG64-28PM (LIME), 710P4-AR, AN-HMA, AN-WMA, WMA-ADVERA) mixtures were determined. The comparison between the test results shows that there is a good relation between SCB CHM and Camera methods; hence, SCB CHM can be used as a reliable test for QA/QC measures.

In addition, a part of the experimental program results were used to develop and calibrate an FE model of the SCB test, and the model was then used to investigate crack propagation in SCB and to predict SCB simulations for experimental results not used in the calibration process. Based on the modeling results of this study, the following conclusions were drawn:

- The XFEM-CZM coupled model successfully simulated the SCB test process as well as the crack propagation.
- The model was successful in predicting the 31.8 and 38.0 mm notch depth SCB testing to a certain extent.
- Crack propagation analysis indicated that SCB failure mechanism is mainly attributed to tensile stresses.
- The XFEM-CZM coupled model provides a suitable numerical tool for representing SCB testing.
- The results of this study indicate that the SCB test holds great potential for measuring the fracture properties of asphalt mixtures.

# 12. RECOMMENDATION:

The results of this study indicated that the SCB test holds great potential as a QA/QC test of the fracture properties of asphalt mixtures. The simplicity of performing the SCB test makes it the preferred test for the QA/QC procedure on the fracture properties of asphalt mixture. In addition, the SCB test can lend itself easily to performance modeling and finite element analysis. However, further studies are recommended in the following areas:

- Assessment of BFT results for higher strain levels (700-1000 micro-strain).
- Sensitivity analysis on different variables such as test temperature and binder content etc. should be evaluated.

## 12. REFERENCE:


[1]. Harvey, J.T., J.A. Deacon, B.W. Tsai, and C.L. Monismith, "Fatigue Performance of Asphalt Concrete Mixes and Its Relationship to Asphalt Concrete Pavement Performance in California", Asphalt Research Program: CAL/APT Program, Institute of Transportation Studies, University of California, Berkeley, October 1995.

[2]. Roberts, F.L., Kandhal, P.S., Brown, E.R., Lee, D., Kennedy, T.W., "Hot Mix Asphalt Materials, Mixture Design and Construction" National Center for Asphalt Technology, Third Edition

[4]. Wagner, M. P., Buttlar, W. G., and Paulino, G. H., "Disk-Shaped Compact Tension Test For Asphalt Concrete" Journal of Experimental Mechanics, v 45, n 3, June, 2005, p 270-277.

[5]. Zhou, F., Hu, S., Scullion, T., Chen, C., Qi, X., and Claros, G. (2007) "Development And Verification Of The Overlay Tester Based Fatigue Cracking Prediction Approach" Journal Of The Association Of Asphalt Paving Technologists, 76.

[6]. Li, X., Marasteanu, M., Kvasnak, A., Bausano, J., Williams, R., and Worel, B., "Factors Study in Low-Temperature Fracture Resistance of Asphalt Concrete" Journal of Materials in Civil Engineering, v 22, n 2, 2010, p 145-152.

[7]. Chiangmai C.N., "Fracture Relation on Asphalt Concrete Mixtures" Thesis, University Of Illinois at Urbana-Champaign, 2010

[8]. Hofman R., Oostcrbaan B., Erkens S., Kooji J., "Semi-Circular Bending Test To Assess The Resistance Against Crack Growth." Road and Hydraulic Engineering Institute, Directorate Public Works and Water Management, Ministry Of Transport, Public Works And Water Management, Delft, Netherland

[9]. Saadeh, S., Eljairi, O., "Development of A Quality Control Test Procedure for Characterizing Fracture Properties of Asphalt Mixtures", California State University of Long Beach, June 2011

[10]. Baoshan Huang, Brian K.Egan, William R.Kingery, "Laboratory Study Of Fatigue Characteristics of HMA Surface Mixtures Containing RAP" TRB 2004 Annual Meeting CD ROM.

[11]. Molenaar, A.A.A.; Scarpas, A.; Liu, X.; Erkens, S.M.J.G. "Semi-Circular Bending Test: Simple but Useful?" Association of Asphalt Paving Technologists-Proceedings Of The Technical Sessions, v 71, 2002, p 794-815

[12]. Mull, M. A., Stuart, K. and Yehia, A., "Fracture Resistance Characterization of Chemically Modified Crumb Rubber Asphalt Pavement," Journal of Materials Science, Vol. 37, pp.557-566, 2002

[13]. Mohammad, N. L., Wu, Z., Aglan, M., "Characterization Of Fracture And Fatigue Resistance On Recycled Polymer-Modified Asphalt Pavements", The 5th RILEM Conference on Pavement Cracking, France, 2004 (In press).

[14]. Mohammad, L. N., Negulescu, I, Wu, Z., Daranga, C., Daly, W.H and Abadie, C.,

"Investigation of the Use of Recycled Polymer Modified Asphalt Binder in Asphalt Concrete Pavements", Asphalt Paving Technology: Association of Asphalt Paving Technologists- Proceedings of the Technical Sessions, v 72, Asphalt Paving Technology 2003, p 551-594

[15]. Molenaar, A., Scarpas, A., Liu, X., and Erkens, S., "Semi-Circular Bending Test: Simple but Useful?" Association of Asphalt Paving Technologists-Proceedings Of The Technical Sessions, v 71, 2002, p 794-815

[16]. Li, X. and Marasteanu, M. "Cohesive Modeling of Fracture in Asphalt Mixtures at Low Temperatures" International Journal of Fracture, v 36, 2005, p 285-308.

[17]. Carpenter, Samuel H., and M. Jansen. "Fatigue Behavior under New Airaraft Loading Conditions." Aircraft/Pavement technology, ASCE, 1997.

[18]. Ghuzlan, K. A., and Carpenter, S. H. (2000). "Energy-Derived, Damage Based Failure Criterion for Fatigue Testing." Transportation Research Record, 1723, Transportation Research Board, Washington, D.C., 141–149.

[19]. Shen, S., and Carpenter, S. H., "An Energy Approach for Airport Pavement Low Damage Fatigue Beha-viour", FAA Worldwide Airport Technology Transfer Conference, Atlantic City, New Jersey, USA, 2007.

[20]. Belytschko, T. and Black, T., "Elastic Crack Growth in Finite Elements with Minimal Remeshing." International Journal for Numerical Methods in Engineering, v 45, n 5, 1999, p 601-620.

[21]. Babuska, I. and Melenk, J., "The Partition of Unity Method." International Journal for Numerical Methods in Engineering, v 40, n 4, 1997, p 727-758.

[22]. Song, J., Areias, P., and Belytschko, T., "A Method for Dynamic Crack and Shear Band Propagation with Phantom Nodes." International Journal for Numerical Methods in Engineering, v 67, 2006, p 868-893.

[23]. Hansbo, A. and Hansbo, P., "A Finite Element Method for the Simulation of Strong and Weak Discontinuities in Solid Mechanics." Jorunal of Computer Methods in Applied Mechanics and Engineering, v 193, 2004, p 3523-3540.

[24]. Ng, K. and Dai, Q., "Investigation of Fracture Behavior of Heterogeneous Infrastructure Materials with Extended-Finite-Element Method and Image Analysis." Journal of Materials in Civil Engineering, v 23, n 12, 2011, p 1662–1671.

[25]. Dugdale, D., "Yielding of steel sheets containing slits." Journal of Mechanics and Physics of Solids, v 8, 1960, p 100-104.

[26]. Aragao, F., and Y-R. Kim. "Characterization of Fracture Properties of Asphalt Mixtures Based on Cohesive Zone Modeling and Digital Image Correlation Technique", Paper presented at the 91st Transportation Research Board Annual Meeting, Washington, D.C., 2010.

[27]. Jamilla L., "Computational Micromechanics Modeling of Damage-Dependent Bituminous Composites Based on Two-way Coupled Multiscale Approach." University of Nebraska-Lincoln, 2011

[28]. Elseifi, M., Mohammad, L., Ying, H., and Cooper, S. "Modeling and Evaluation of the Cracking Resistance of Asphalt Mixtures Using the Semi-Circular Bending Test at Intermediate Temperatures" Paper presented at the 91st Association of Asphalt Pavement Technologists Annual Meeting, Austin, TX, 2012.

[29]. Abu Al-Rub, R., Masad, E., and Huang, C., "Improving the Sustainability of Asphalt Pavements through Developing a Predictive Model with Fundamental Material Properties," Final Report submitted to Southwest University Transportation Center, 2009.